International Journal of Nanomedicine

Dovepress
Taylor & Francis Group

Open Access Full Text Article

ORIGINAL RESEARCH

Tumor Microenvironment Responsive Key Nanomicelles for Effective Against Invasion and Metastasis in Ovarian Cancer Using Mice Model

Yang Liu[1,2], Liang Kong[1,2], Yang Yu[1,2], Juan Zang[1,2], Lu Zhang[1,2], Rui-Bo Guo[1,2], Shu-Tong Li[1,2], Lan Cheng[1,2], Xue-Tao Li[1,2], You-Qiang Chen[1,2]

[1]School of Pharmacy, Liaoning University of Traditional Chinese Medicine, Dalian, 116600, People's Republic of China; [2]Shenyang Key Laboratory of Chinese Medicine Targeted Delivery Key Laboratory, Shenyang, 110847, People's Republic of China

Correspondence: Xue-Tao Li; You-Qiang Chen, School of Pharmacy, Liaoning University of Traditional Chinese Medicine, Shengming 1 Road 77, Double D Port, Dalian, 116600, People's Republic of China, Tel +86411 8589 0170, Fax +86411 8589 0128, Email lixuetao1979@163.com; 89427765@qq.com

Background: Ovarian cancer is difficult to detect in its early stages, and it has a high potential for invasion and metastasis, along with a high rate of recurrence. These factors contribute to the poor prognosis and reduced survival times for patients with this disease. The effectiveness of conventional chemoradiotherapy remains limited. Nano-particles, as a novel drug delivery system, have significant potential for improving therapeutic efficacy and overcoming these challenges.

Methods: According to the high expression level of matrix metalloproteinase-2 (MMP-2) in the tumor microenvironment, MMP-2 responsive nano-particles (PVGLIG-MTX-D/T-NMs) containing docetaxel and triptolide were prepared by the thin-film dispersion method. The synergistic effect between docetaxel and triptolide was systematically investigated, the ratio of the two drugs was optimized, and the physicochemical properties of the nano-particles and their ability to inhibit ovarian cancer cell growth and metastasis were evaluated in vitro and in vivo.

Results: PVGLIG-MTX-D/T-NMs enhanced the targeting, stability, and bioavailability of the drug, while reducing the dose and toxicity. In addition, by regulating the expression levels of E-Cadherin, N-Cadherin, matrix metalloproteinases (MMPs), hypoxia-inducible factor 1-alpha (HIF-1α), and vascular endothelial growth factor (VEGF), it exhibited an inhibitory effect on epithelial-mesenchymal transformation (EMT) and tumor cell angiogenesis, and effectively inhibited the invasion and metastasis of ovarian cancer cells.

Conclusion: PVGLIG-MTX-D/T-NMs achieved passive targeting of tumor sites by enhancing permeability and retention (EPR) effects. Subsequently, the uptake of the drug by tumor cells was enhanced by MMP-2 responsiveness and the modification of methotrexate targeting ligands. By regulating the expression levels of invasion- and metastasis-related proteins in tumor tissues, the nano-particles affected the EMT process, inhibited tumor angiogenesis, and suppressed the malignant potential of invasion and metastasis in ovarian cancer. These findings provided a new direction for further exploration of tumor-targeted therapy.

Keywords: nano-drug delivery system, tumor microenvironment, docetaxel, triptolide, epithelial mesenchymal transition, angiogenesis

Introduction

Ovarian cancer is one of the three common malignant tumors in gynecology, with the highest mortality rate among gynecologic tumors, seriously threatening women's health.[1] Due to its deep location in the peritoneal cavity, ovarian cancer mainly presents with subtle early symptoms, making early detection challenging. Consequently, approximately two-thirds of patients are diagnosed at advanced stages.[2] At present, surgical intervention, chemotherapy, targeted therapy inhibiting angiogenesis, and adenosine diphosphate ribose polymerase (PARP) inhibitors are the primary modalities for managing ovarian cancer.[3] While a small subset of patients may achieve cure through surgery alone, the majority require combined treatment approaches, such as surgery plus chemotherapy. Difficulties in early diagnosis,

Received: 22 March 2024
Accepted: 15 December 2024
Published: 7 January 2025

metastasis, and drug resistance are crucial factors, leading to treatment failure and death in patients with ovarian cancer.[4,5] Paclitaxel (PTX), docetaxel (DTX), doxorubicin, methotrexate (MTX), and platinum agents are frequently utilized in the management of gynecological malignancies.[6]

Docetaxel (DTX), a widely used antitumor drug, primarily exerts its inhibitory effects on tumor cell division and growth by disrupting microtubule dynamics.[7] However, due to the complexity of cancer as a disease, monotherapy mainly falls in achieving satisfactory treatment outcomes. Therefore, combination therapy involving multiple drugs targeting different pathways has emerged as an effective approach for combating cancer and minimizing the risk of drug resistance development.[8] Numerous preclinical studies have demonstrated the superiority of combination strategies in overcoming or delaying drug resistance development.[9] The success of such strategies relies on careful selection of drugs and optimized delivery methods.

Triptolide (TPL), a unique compound derived from the plant *Tripterygium wilfordii*, is the most active and toxic component of its monomeric form. It exhibits immunosuppressive and anti-inflammatory effects, making it a valuable therapeutic option for various immune-related diseases, including rheumatoid arthritis, systemic lupus erythematosus, and nephritis.[10] Recent studies have demonstrated TPL's potential as an antitumor agent by inhibiting tumor cell growth particularly in lung cancer, breast cancer, osteosarcoma, prostate cancer, neuroblastoma, and gastrointestinal tumors. Additionally, TPL synergistically enhances the efficacy of chemotherapeutic agents, such as cisplatin, to overcome drug resistance in ovarian cancer, lung cancer, breast cancer, and bladder cancer.[11]

The present study aimed to investigate the potential of combining DTX and TPL for treating ovarian cancer. Similar to other tumors, effective treatment of ovarian cancer requires targeting tumor cells while minimizing harm to normal cells, particularly vital organs, in order to avoid severe damage.[12] In contrast to other tumors, preserving fertility and protecting the unborn child are noteworthy when treating ovarian cancer.[13] However, both DTX and TPL exhibit significant toxic side effects during chemotherapy. Common adverse reactions associated with DTX include myelosuppression, allergic reactions, fluid retention, and gastrointestinal disturbances. Myelosuppression is primarily characterized by the decreased levels of white blood cells, red blood cells, platelets, and neutrophils.[14] Patients may experience symptoms, such as pale complexion, dizziness, headaches, and fatigue due to anemia. Additionally, symptoms, involving bleeding from the skin or mucosa, gum bleeding, and nosebleeds, may occur. TPL's active ingredient also exhibits potent toxicity to the reproductive system, liver, and kidneys.[15] Additionally, limited solubility and a short in vivo half-life further restrict their clinical application.[16] Therefore, the development of an efficient delivery system for DTX plus TPL is essential to ensure their effective anticancer effects while reducing associated side effects.

The nano-drug delivery system is a cutting-edge technology that miniaturizes the drug carrier to the nano-scale, enabling targeted delivery of drugs to specific tissues or cells. This enhances drug efficacy and minimizes side effects.[17] Commonly used nano-carriers include polymer nano-particles, polymer micelles, and liposomes. This innovative approach improves solubility for insoluble drugs while prolonging blood circulation through controlled release kinetics. It also enhances targeting precision and bioavailability of therapeutic agents.[18] Consequently, it reduces the required dosage while mitigating toxicities associated with systemic exposure to drugs to optimize treatment outcomes and ensure patient safety. Notably, this can primarily be attributed to the passive diffusion of nano-particles into tumor regions via EPR effect, followed by controlled drug release in the unique tumor microenvironment (TME) or through exploitation of overexpressed enzymes or proteins in these areas. Furthermore, active targeting groups, including peptides, carbohydrate derivatives, transporter targets, and antibodies, can also be modified on the surface of nano-particles to increase uptake by tumor cells and play a noticeable therapeutic role.[19]

In recent years, therapeutic strategies that target the TME have emerged as a promising approach for cancer treatment.[20] TME refers to the complex and diverse multicellular environment where tumors develop, involving extracellular matrix (ECM) components and stromal cells.[21] The TME plays a pivotal role in ovarian cancer development by serving as a critical regulatory barrier against tumor metastasis while influencing tumor progression and metastatic potential.[22] Therefore, it represents a potential therapeutic target for managing ovarian cancer. In contrast to most solid tumors that spread via lymphatic or hematogenous pathways, ovarian cancer cells can directly spread into the peritoneum, interact with the mesothelial cells lining the peritoneum, and subsequently invade the basement membrane and spread to the ECM to form metastatic implants.[23] Matrix metalloproteinases (MMPs) are a class of enzymes, playing

roles in degrading and remodeling ECM. Over the recent decades, researchers have demonstrated that high levels of MMPs in cancer, especially MMP2 and MMP9, can promote invasion, metastasis, and angiogenesis of various tumor cells by providing pathways through degradation of matrix proteins, thereby enabling tumor cells to cross the stroma and invade surrounding tissues and blood vessels.[24]

Methotrexate (MTX) is a broad-spectrum antitumor agent that competitively inhibits dihydrofolate reductase, thereby suppressing DNA and RNA synthesis and exerting an anticancer effect.[25] Furthermore, MTX exhibits structural similarity to folic acid and serves as a representative derivative of this compound. By binding to highly expressed folic acid receptors on the surface of tumor cells, MTX can effectively target tumor sites.[26] Studies have demonstrated that incorporating MTX as a targeting ligand on the surface of nano-micelles and facilitating their endocytosis through folate receptors may enhance drug concentration in tumor tissues, leading to the improved therapeutic outcomes.[27]

Based on the aforementioned background, in the present study, a step-targeted nano-micelle system (PVGLIG-MTX -D/T-NMs) responsive to MMP-2 was developed. The hydrophobic core of the nano-micelles encapsulated DTX and TPL. PEG_{5000} was conjugated to the outer end of the MMP-2 sensitive peptide, positioning it at the outermost layer of the nano-micelle to form a hydrated membrane coating. This coating could enhance EPR effect while concealing the active targeting ligand MTX specific for ovarian cancer cells. Consequently, drug uptake by normal cells was minimized, leading to a reduction in toxic side effects. Upon passive targeting of nano-micelles to tumor sites through EPR effect, overexpressed MMP-2 could cleave the MMP-2 sensitive peptide, triggering a cascade of events that result in the enzymatic degradation of the PEG_{5000} hydrated layer and the subsequent exposure of the MTX-targeting ligand. The uptake of MTX-D/T-NMs by ovarian cancer cells could be enhanced through folic acid receptor-mediated endocytosis, ultimately leading to the dissolution of micelles and release of drugs in the intracellular environment to achieve therapeutic efficacy. This nano-micelle system could effectively reduce the toxicities and side effects associated with free drugs, thereby facilitating efficient targeted drug delivery.

Materials and Methods

Docetaxel, p-glycoprotein inhibitor D-alpha-Vitamin E polyethylene glycol succinate ($TPGS_{1000}$), EdU-488 cell proliferation assay kit, one-step TUNEL apoptosis assay kit, and hematoxylin and eosin (H&E) staining kit were purchased from Dalian Meilun Biotechnology Co., Ltd. (Dalian, Liaoning, China). Triptolide was obtained from Chengdu Glip Biotechnology Co., Ltd. (Chengdu, Sichuan, China). Soluplus was sourced from BASF (Germany). DSPE-PEG_{2000} was purchased from NOF (Tokyo, Japan). DSPE-PEG_{2000}-PVGLIG-PEG_{5000} and DPE-PEG_{2000}-MTX were synthesized by Xi'an Ruixi Biotechnology Co., Ltd. (Xi'an, Shaanxi, China). DSPE-PEG_{2000} was also synthesized by Shanghai Peptide Co., Ltd. (Shanghai, China). Matrigel was obtained from BD Biosciences Co., Ltd. (San Jose, California, USA). 40,6-diamino-2-phenylindole (DAPI), albumin (ALB) test kit, alanine aminotransferase (ALT) test kit, aspartate aminotransferase (AST) test kit, and alkaline phosphatase (AKP) test kit were acquired from Solarbio Technology Co., Ltd. (Beijing, China). Cell Counting Kit-8, cell viability (live and dead cell staining) kits, and apoptosis-Hoechst staining kits were provided by EallBio Life Sciences, Inc. (Beijing, China). 1.1-octacosalkyl-3,3,3,3-tetramethylindole tricarbon cyanide iodide (DiR) was sourced from Nanjing Kaiji Biotechnology Development Co., Ltd. (Nanjing, Jiangsu, China). Ki-67, E-Cadherin, N-Cadherin, MMP-2, MMP-9, HIF-1α, and VEGFA antibodies were purchased from Abcam, Inc. (Cambridge, MA, USA). All other reagents used are analytical grade, and the water is pure water.

The SK-OV-3 cells were purchased from the Institute of Basic Medicine, Chinese Academy of Medical Sciences (Beijing, China). The cells were cultured in MCCOY's 5A medium (Beijing Solarbio Technology Co., Ltd., Beijing, China) supplemented with 10% fetal bovine serum and 1% penicillin/streptomycin at 37 °C and 5% CO_2. Female BALB/c nude mice, weighing 20 ± 2 g, were obtained from Liaoning Changsheng Biotechnology Co., Ltd. (Benxi, Liaoning, China). The BALB/c nude mice were maintained at a constant temperature of 22–24°C and humidity of 55–60% in the Laboratory Animal Center of Liaoning University of Traditional Chinese Medicine. The experimental program was approved by the Animal Research Ethics Committee of Liaoning University of Traditional Chinese Medicine, and all procedures were conducted in strict accordance with the "Guidelines for the Welfare and Ethics of Laboratory Animals" (GB/T 35892–2018), which is the national standard of China for the care and use of laboratory animals.

The Synthesis of Nanomicelles by Thin-Film Dispersion Method

MMP-2 responsive step-targeting nanomicelles (PVGLIG-MTX-D/T-NMs) containing docetaxel and triptolide were prepared using the thin-film dispersion method. 40mg Soluplus, 20mg $TPGS_{1000}$, 2mg DSPE-PEG_{2000}, 2mg DSPE-PEG_{2000}-PVGLIG-PEG_{5000}, 2mg DSPE-PEG_{2000}-MTX, 2mg DTX, and 4.46μg TPL were transferred into a 15mL centrifuge tube. The aforementioned materials were dissolved in methanol and transferred to a round-bottom flask with a capacity of 50 mL which was then evaporated under reduced pressure at 40°C using a water bath until forming a film at the bottom of the flask. Afterwards, 5mL PBS solution was added for hydration followed by extrusion twice through the microporous filter membrane with pore size being 0.22 μm to obtain PVGLIG-MTX-D/T-NMs.

The fluorescent probe coumarin (Cou) was chosen instead of DTX and TPL to assess the cellular uptake of micelles in vitro. In vivo, DiR was employed as a fluorescent probe to analyze the circulation time and tumor targeting of nanomicelles. The preparation method for these two micelles remains consistent with the aforementioned procedure, except that Cou or DiR is substituted for DTX and TPL.

The Examination of Nanomicelles by Different Technologies

The characteristics of nanomicelles were observed by transmission electron microscopy. The micelles were diluted in phosphate-buffered saline (PBS), one drop was placed on the copper mesh and allowed to dry naturally. The morphological characteristics of the micelles were observed by transmission electron microscopy (TEM, Tecnai G220ST, FEICo., Tokyo, Japan). The particle size, polydispersity index (PDI) and zeta potential values of PVGLIG-MTX-D/T-NMs and MTX-D/T-NMs were measured using a dynamic light scattering (DLS) analyzer (Malvern Instruments, NanoZS90, UK). The contents of DTX and TPL in liposome suspension before and after column were determined by high performance liquid chromatography (HPLC) with UV absorption detector. The mobile phase of DTX was acetonitrile-water (63:37, *V/V*). Agilent ZORBAX SB-Aq C18 column (250 mm × 4.6 mm, 5 μm) was used for the determination. The detection wavelength was 230 nm. The mobile phase of TPL was methanol-0.1% phosphoric acid solution (45:55, *V/V*) and the detection wavelength was 215 nm. The formula of Encapsulation efficiency (EE) and drug load (DL) is as follows:

EE % = (peak area of drug after column/peak area of drug before column) × 100%

DL%= (amount of drug in micelle/total micelle) × 100%

Measurement of the Critical Micelle Concentration Utilizing Pyrene as a Fluorescent Indicator

Determination of micellar Critical Micelle Concentration (CMC) by pyrene as a fluorescent probe. The 40.4 mg pyrene was accurately weighed and placed in a 10mL volumetric bottle, then the volume was fixed with acetone, and then diluted 100 times to obtain 2×10^{-4} mol/L reserve solution. Blank-NMs was prepared into micellar solutions of different concentrations. Add a reserve solution of 80 μL pyrene to the test tube and let dry naturally overnight away from light. Use pipette to absorb the above micellar solutions of different concentrations of 8 mL each, add to the test tube, so that the final concentration of pyrene is 2×10^{-6} mol/L. Add 200ul to each hole of the 96-well plate. The fluorescence values at 372 nm and 383 nm were measured by fluorescence spectrometer. The critical aggregation concentration was calculated by cross plotting logC of I_{372}/I_{383} to the sample concentration C (mg/mL).

The Stability of Drug-Loaded Nanomicelles

PVGLIG-MTX-D/T-NMs was prepared and divided into 2 mL/tube. 3 parallel samples were prepared for each. The solution was stored in a refrigerator at 4°C, then the solution was taken every 7 days for DLS particle size determination, and the change of the encapsulation efficiency of DTX and TPL in different micellar preparations was determined by HPLC. The storage stability of nanomicelles was investigated by observing the changes of particle size and encapsulation efficiency with time.

Assessment of Enzymatic Sensitivity in Nanomicelles

The enzyme sensitivity of PVGLIG-MTX-D/T-NMs was assessed through a degradation test using MMP-2 sensitive peptides. A volume of 1 mL of nanomicellar solution was taken and supplemented with 10 μL of MMP-2 mother liquor (concentration: 500 μg/mL). Another group of nanomicelles was treated with 10 μL PBS. Incubation at 37 °C for 2h followed. Dynamic light scattering (DLS) analysis was employed to evaluate the size reduction of micelles, thereby assessing their stimulus-responsive behavior.

Drug Release from Nanomicelles in vitro

The in vitro drug release experiment was carried out by dialysis bag method. PBS solution containing 10% FBS and 500 μg/mL MMP-2 was used as the release medium to simulate the release behavior in vivo. 1mL nanomicelles were added into the dialysis bag and sealed so that the dialysis bag was floating in 100 mL of the release medium, and the drug release was promoted by magnetic stirring away from light. At 2, 8, 16, 32, 48 and 72 h, 0.5 mL of the release medium was absorbed from the beaker as a sample, and the equal-volume fresh medium was added. HPLC method was used to detect drug concentration in the release solution, and the in vitro release rate was calculated according to the following formula:

In vitro release rate %= (drug content in the release medium/drug dosage) × 100%

Evaluation of Synergistic Effects Between Docetaxel and Triptolide Using SynergyFinder Analysis

The SK-OV-3 cells were seeded in a 96-well plate at a density of 1.5×10^4 cells/ well, followed by drug addition using the checkerboard method after 12h of incubation. The concentrations of free DTX and free TPL were determined based on established references and preliminary experiments. Subsequently, the cells were cultured for an additional 48h post-treatment, and cell viability was assessed using Cell Counting Kit-8 kits. Synergy analysis was performed utilizing the online SynergyFinder software (https://synergyfinder.fimm.fi), employing the response surface model and zero interaction effect (ZIP) drug score with an "inhibition index" (=100 - cell vitality inhibition index). A ZIP Synergy score greater than 0 indicates synergy, while a score exceeding 10 signifies strong synergistic effects.[28]

Evaluation of Cytotoxic Effects of Nanomicelles on Ovarian Cancer Cells

The SK-OV-3 cells were seeded in a 96-well plate at a density of 1.5×10^4 cells/well. After being incubated for 12h, the respective micelle groups were added. After culturing the cells for 48h, cell viability was assessed using the Cell Counting Kit-8 (CCK-8). The IC50 values were calculated using GraphPad Prism 9.0 software. To determine cell viability, we employed a live and dead cell staining assay kit that allowed simultaneous observation of live cells (yellow-green fluorescence) and dead cells (red fluorescence) under a fluorescence microscope with an excitation wavelength of approximately 490 nm.

Assessment of in vitro Hemolytic Activity of Nanomicelles

The freshly collected blood was placed in a centrifuge tube containing 2% heparin sodium (with a volume ratio of 9:1 for blood to 2% heparin sodium), mixed with ten times the amount of normal saline, and then centrifuged at 4°C, 1500 rpm for 10 minutes. Subsequently, the supernatant was discarded, and the precipitated red blood cells at the bottom were collected and washed three times using the aforementioned method until the supernatant became colorless or showed no obvious redness after centrifugation. The bottom red blood cells were prepared into a red blood cell suspension with a volume ratio of 2% using normal saline. The PVGLIG-MTX-D/T-NMs solution was diluted to an isotonic concentration of 10 mg/mL. Next, 500 μL of red cell suspension was placed in a 1.5mL centrifuge tube, followed by addition of different volumes (10 μL, 20 μL, 40 μL, 60 μL, and 80 μL) of PVGLIG-MTX-D/T-NMs sample solutions along with 100 μL normal saline to ensure that the final volume reached 1 mL. Furthermore, the negative control group used normal saline while double steaming water served as positive control group; four groups of parallel samples were set up. All groups were incubated at 37°C for 4 h, followed by centrifugation at 1500 rpm for 10 minutes.The absorbance

measurements for hemoglobin in supernatant were taken at 540 nm wavelength using an enzyme-labeler, and absorbance values for PVGLIG-MTX-D/T-NMs at different concentrations (0.1, 0.2, 0.4, 0.6, and 0.8 mg/mL) were recorded. Hemolysis analysis was performed on PVGLIG-MTX/T-NMs samples with varying concentrations (1 mg/mL).

The hemolysis rate is calculated according to the following formula:

Hemolysis rate (%) = (A_{sample} -$A_{negative}$) / ($A_{positive}$ -$A_{negative}$)

Where, A_{sample} represents the absorbance measured from the supernatant obtained after co-incubation with the test sample; $A_{negative}$ represents the absorbance from the supernatant after incubating red blood cells with physiological saline; $A_{positive}$ represents the absorbance from red blood cells incubated with double-distilled water.

Investigation of Folate Receptor-Mediated Endocytosis in SK-OV-3 Cells

To investigate the endocytosis of nanoparticles mediated by folate receptors in SK-OV-3 cells, we employed laser confocal microscopy to examine the expression of folate receptors on the surface of SK-OV-3 cells and to assess the co-localization of nanoparticles within the cells. The experimental procedure was as follows: 1×10^4 SK-OV-3 cells were seeded in a round glass dish and allowed to attach overnight. Subsequently, different micelles loaded with coumarin (Cou-NMS, MTX-Cou-NMs, and MTX-Cou-NMs +FA) were added at a final concentration of 2 μM. After co-incubation for 4 h, the cells were washed and fixed. Next, the cell samples were incubated with a blocking solution (5% FBS) at room temperature for 1h followed by overnight incubation with anti-folic acid antibody at 4°C. Following repeated washing with PBS, Cy5-labeled secondary antibodies were applied to the samples at room temperature for 1h while DAPI was used for nuclear staining. Finally, the cell samples were observed and imaged using confocal laser microscopy (Leica, Germany).

Analysis of Nanomicelle Uptake in SK-OV-3 Cells

The uptake of different micelles in SK-OV-3 cells was qualitatively analyzed using confocal laser microscopy. SK-OV-3 cells at the logarithmic growth stage were digested, diluted, and inoculated into a 6-well plate at a density of 1×10^5/well. Three parallel double wells were set up and incubated in an incubator at 37°C, 5% CO_2, and 90% relative humidity for 24h. Coumarin-containing Cou-NMs, MTX-Cou-NMs PVGLIG-MTX-Cou-NMs+MMP2 were added to the 6-well plate and incubated under various conditions. The coumarin concentrations were maintained at 2μM for different durations (1, 2, and 3h), as well as at different concentrations (1, 2, and 4 μM) for a duration of 2h. After washing with PBS buffer three times, the cells were fixed with a solution containing 4% paraformaldehyde for ten minutes. DAPI staining solution was used to stain the nuclei for six minutes before observing the distribution of fluorescence within the cells using laser confocal microscopy.

After treatment with the same method, the cells were subjected to triple PBS buffer washes, trypsin digestion, centrifugation, and subsequent resuspension in 500 μL of PBS. The average fluorescence intensity of coumarin uptake by SK-OV-3 cells was determined under different administration times and concentrations using FACScan flow cytometry.

Inhibition of Cell Proliferation in SK-OV-3 Cells by Nanomicelles

The SK-OV-3 cells were seeded at a density of 1×10^4/well in 48-well plates and cultured overnight until reaching confluency. Subsequently, different nanomicelles were added to each well to achieve a final DTX concentration of 1.744 μM/well. Blank-lips were used as the negative control, with three replicates set for each group. Then, the cells were processed according to the instructions provided with the EDU kit. Fluorescence microscopy was employed to observe and capture images, while Image J software was utilized for cell counting and determination of the percentage of positively stained cells.

Positive cell rate = number of positive cells/total cell number ×100%

Assessment of Cell Apoptosis Induced by Nanomicelles

The SK-OV-3 cells were seeded in 48-well plates at a density of 1×10^4 cells/well and incubated overnight for drug treatment. Following a 48h incubation period, the SK-OV-3 cells were subjected to Hoechst 33342 apoptosis staining using a fluorescence microscopy imaging system.

SK-OV-3 cells with a density of 1×10^5/ well were inoculated into the 6-well plate, and each group of nanomicelles was added when the length reached 70%. After culture for 48h, the cells were collected and Annexin V-FITC and PI were added for double staining according to the AnnexinV/PI double dyeing kit instructions. The reaction was carried out at room temperature for 15 min and the apoptosis of SK-OV-3 cells was detected by flow cytometry within 1h.

Apoptosis rate = (number of early apoptotic cells + number of late apoptotic cells)/ total number of cells ×100%

In vitro Assessment of Nanomicelle Efficacy on Ovarian Cancer Cells Invasion and Migration

The inhibitory effects of various micelles on SK-OV-3 cell wound healing were investigated using a scratch test. Cells were seeded in 6-well plates at a concentration of 1×10^5 cells/well. After overnight incubation, a straight line was created within the cell monolayer using the tip of a sterile 20 μL pipette with consistent intensity and angle to ensure uniformity in line thickness. The detached cells were washed away with PBS, followed by addition of fresh 5A medium containing different nanomicelles. Subsequently, an inverted microscope was employed to observe the rate of scratch closure at different time points post-treatment, and images were captured for analysis. The area of the scratch was quantitatively analyzed using Image J software. The formula used for calculating the wound healing rate is as follows:

Wound healing rate %= $(1- A_t /A_0) \times100\%$, where A_t represented the scratch area measured at 12h or 24h, and A_0 represented the scratch area measured at 0 h.

The cell migration experiment was conducted using a Transwell co-culture chamber. In the lower chamber of the Transwell, 600 μL of 5A medium containing FBS was added, while in the upper chamber, 20 μL of different nanomicelles and 180 μL of cell suspension were added, which overhung by 5A medium without FBS. The cell density per well was maintained at 2×10^4 cells/well. After incubation at 37°C for 24 h, the upper chamber was removed and swabbed with PBS four times. Subsequently, it was fixed with a solution of 4% paraformaldehyde for 20 min and stained with a solution of crystal violet (0.4%) at room temperature for a duration of ten minutes. Unbound crystal violet dye was washed away using PBS followed by air-drying at room temperature. The membrane was observed under an inverted microscope and images were captured accordingly. Cell counting in these images was performed using Image J software to determine cell mobility as calculated by the following formula.

Mobility (%) = Number of cells in preparation group/number of cells in blank control group × 100%

For the cell invasion experiment, the 20 μL sterile pipette tip, transwell chamber and Ep tube were pre-cooled at 4°C in advance. The Transwell chamber was then coated with matrix glue on ice (the matrix glue was diluted with serum-free medium at a ratio of 1:4). Subsequently, 180 μL of cell suspension was added into the chamber based on a density of 3×10^4 cells/mL. All other procedures remained consistent with those used in the cell migration experiment.

Invasion rate (%) = number of cells in preparation group/number of cells in blank control group × 100%

Inhibition of Vasculogenic Mimicry Channel Formation in SK-OV-3 Cells by Nanomicelles

Add 50 μL of matrix glue to each well of the 96-well plate, ensuring thorough mixing to eliminate any bubbles. Immediately transfer the plate to a cell incubator set at 37 °C for 30 min to allow solidification of the matrix glue. SK-OV -3 cells were then seeded into the aforementioned wells at a concentration of 1.5×10^4 cells/well, followed by addition of nanomicelles with different formulations into each well. Incubate for an additional 4 h and observe micelle-induced disruption on mimicry angiogenesis using an inverted microscope. Employ Image J software for analysis of nodes, junctions, branches, and segments within the mimicry vessels.

Establishment of Xenograft Mouse Model of Ovarian Cancer

To assess the in vivo tumor targeting ability and drug distribution of PVGLIG-MTX-D/T-NMs, a xenograft mouse model of SK-OV-3 cells was established by inoculating 1.5×10^6 suspended SK-OV-3 cells in 200 μL medium onto the left armpit of BALB/c nude mice's forelimb. Subsequent experiments were conducted when the tumor volume reached approximately 200 mm^3.

In vivo Tumor Targeting and Drug Distribution of Nanomicelles

In order to assess the tumor targeting ability and in vivo drug distribution of different nanomicelles, tumor-bearing mice were randomly divided into 5 groups (n=3). Each group was administered with nanomicelles containing the near-infrared fluorescent probe DiR for tracking the distribution of nanocarriers in vivo. The administration groups included normal saline (blank control), Free DiR, DIR-NMs, MTX-DiR-NMs, and PVGLIG-MTX-DiR-NMs. All administrations had an equal dose of DiR at 1μg/piece. Whole-body fluorescence imaging was performed on isoflurane-anesthetized mice at excitation/emission wavelength of 748/780 nm using IVScope 8200 in vivo imaging system (Clinx science instruments Co.,Ltd) at 3, 6, 12, 24, 48 and 72 h post-administration to visualize the distribution of various nanomicelles.

In vivo Safety and Pharmacodynamic Assessment of Nanomicelles in Ovarian Cancer Mouse Model

In vivo safety and pharmacodynamic evaluation of nano micelles were conducted using a mouse model of ovarian cancer xenotransplantation, following the aforementioned methods. Once the tumor volume reached 200 mm^3, the mice were randomly divided into 5 groups (n=12), with 6 mice used solely for statistical survival curve analysis and another 6 used exclusively for in vivo safety and pharmacodynamic assessment. In the blank control group, a mixture of 150 μL PBS and DMSO was injected into the tail vein every two days (volume ratio 19:1). The remaining groups received an intravenous administration of a preparation solution containing 150 μL at a dose equivalent to DTX 3mg/kg every two days. Survival curves were monitored for all groups up to day 40 post-treatment. The treatment period lasted for 12 days. Mouse weight and tumor volume were recorded after each injection during this period, allowing calculation of tumor inhibition rate.

Tumor volume V (mm^3) = tumor length × tumor $width^2$ /2.

Tumor inhibition rate (%) = (1- average tumor volume of each experimental group/average tumor volume of blank control group)×100%.

Two days after the final administration, orbital blood was collected from mice for liver function examination, including albumin (ALB), alanine aminotransferase (ALT), aspartate aminotransferase (AST) and alkaline phosphatase (AKP). Subsequently, tumors and major organs (heart, liver, spleen, lung and kidney) were completely removed from euthanized mice and fixed in 4% paraformaldehyde for 24h. The fixed tissues were sectioned into small pieces and embedded in paraffin wax. Each tissue was then cut into 5μm thick slices using a paraffin microtome. Major organs of the mice were stained with H&E to evaluate the safety of different formulations. H&E staining of tumor tissue was used to evaluate the destructive effect of different preparations on axillary tumor tissue in tumor-bearing mice. TUNEL kit was utilized to detect apoptosis-inducing effects of each preparation on tumor tissue in vivo. Immunohistochemistry was performed to determine Ki-67 expression levels for investigating proliferation rates of tumor cells while immunofluorescence staining investigated E-Cadherin, N-Cadherin, MMP-2, MMP-9, HIF-1α, and VEGFA expressions.

Statistical Analysis

Experimental data were analyzed using GraphPad Prism 9.0 software, and results were presented as mean ± standard deviation (mean±SD) of at least three experiments. Statistical significance was determined by one-way analysis of variance (ANOVA) or non-parametric test with $*P < 0.05$ considered significant.

Results and Discussion

The direct images obtained through transmission electron microscopy (TEM) provide an effective method for examining the structural characteristics of polymers. Figure 1A and B clearly depict the homogeneous, sphere-like micelle structures of MTX-D/T-NMs and PVGLIG-MTX-D/T-NMs, respectively, self-assembled in aqueous solution. The average particle size of MTX-D/T-NMs (Figure 1C) was determined to be 71.72±1.59 nm, with a low polydispersity index (PDI) of 0.02 ±0.01, and exhibited a Zeta potential value of −1.33±0.15 mV (Figure 1D). Similarly, PVGLIG-MTX-D/T-NMs displayed an average particle size of 80.80±0.54 nm (Figure 1E), a PDI value of 0.09 ±0.01, and a Zeta potential value of −1.40 ±0.20 mV (Figure 1F). These well-defined spherical nano-particles, with uniform sizes and narrow

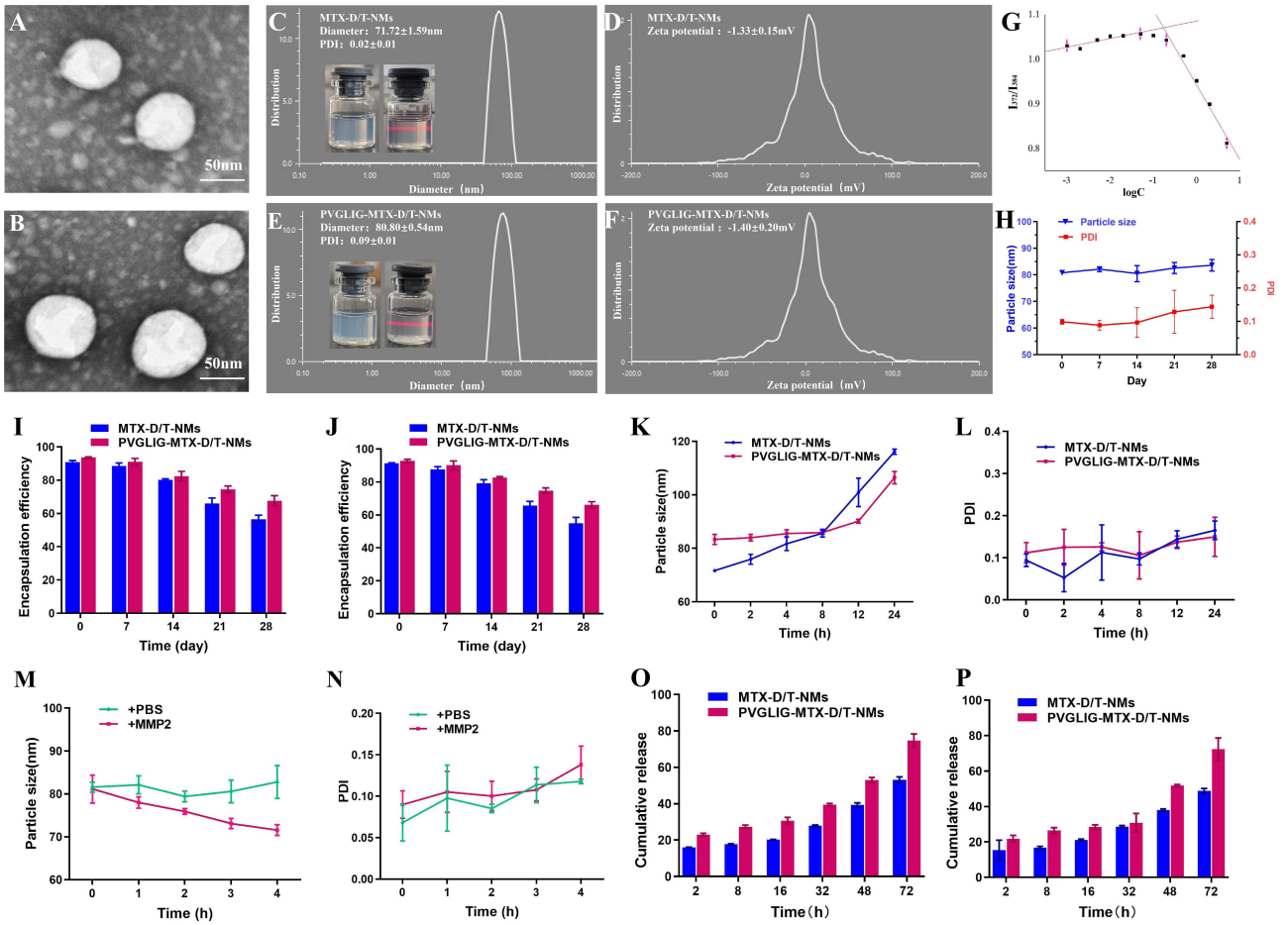

Figure 1 Characterization and stability of micelles. (**A**) Transmission electron microscope image of MTX-D/T-NMs; (**B**) Transmission electron microscope image of PVGLIG-MTX-D/T-NMs; (**C** and **D**) Particle size distribution and zeta potential distribution of MTX-D/T-NMs; (**E** and **F**) Particle size distribution and zeta potential distribution of PVGLIG-MTX-D/T-NMs; (**G**) Critical micelle concentration of PVGLIG-MTX-D/T-NMs; (**H**) Changes in particle size and PDI of PVGLIG-MTX-D/T-NMs stored at 4°C for 28 days; (**I**) Changes in the encapsulation rate of DTX in different micelle preparations at 4°C; (**J**) Changes of the encapsulation rate of TPL in different micellar preparations at 4°C; (**K** and **L**) Changes in particle size and PDI of different nanomicelles in 10% serum; (**M** and **N**) Evaluation of MMP-2 responsiveness of PVGLIG-MTX-D/T-NMs; (**O**) the release rate of DTX in different micelles at 37°C; (**P**) the release rate of TPL in different nanomicelles at 37°C. Data are expressed as mean ± SD deviation (n=3).

distribution (PDI<0.200), significantly contribute to the enhanced penetration and retention effects, as well as cellular endocytosis. The surface of the nano-micelles is negatively charged, leading to a reduction in non-specific adsorption of plasma proteins and an extension in the half-life of blood circulation. Moreover, both MTX-D/T-NMs and PVGLIG-MTX-D/T-NMs solutions exhibit clear and transparent colors with evident Tindahl phenomenon upon standing at room temperature. The encapsulation rate of PVGLIG-MTX-D/T-NMs reached 93.18±0.76%, while the drug loading was measured at 3.1±0.03%. The results obtained from pyrene fluorescence method are depicted in Figure 1G, revealing a critical micelle concentration of 0.174 mg/mL, signifying promising self-assembly ability of the micelles studied in water-based media where stable micelle structures can be formed even at low mass concentrations. PVGLIG-MTX-D/T-NMs demonstrated minimal variations in particle size and PDI value following 28 days of storage at 4 °C, indicating their excellent storage capability (Figure 1H). Changes in encapsulation rates for different nano-micelles stored at 4 °C for 28 days are presented in Figure 1I and J. As storage time increased, the encapsulation rate decreased, while it remained higher for PVGLIG-MTX-D/T-NMs compared with MTX-D/T-NMs, suggesting superior stability of PVGLIG-MTX-D/T-NMs.

The nano-carriers must exhibit stability during the drug delivery process. Upon entering tumor cells, the nano-carriers underwent destabilization and prompt drug release, thereby achieving optimal drug delivery efficacy. Figure 1K and L illustrate the variations in particle size and PDI of different nano-micelles in a 10% serum environment. Over time, the particle size of

https://doi.org/10.2147/IJN.S470219

MTX-D/T-NMs was noticeably elevated, which was significantly higher compared with PVGLIG-MTX-D/T-NMs. This discrepancy could be attributed to the presence of a hydrophilic invisible layer on the surface of PVGLIG-MTX-D/T-NMs, enhancing its stability in serum and facilitating prolonged circulation in in vivo systems. Evaluation of the results for MMP-2 responsiveness (Figure 1M and N) demonstrated that PBS addition had minimal impact on the mean particle size of PVGLIG-MTX-D/T-NMs; however, upon adding MMP-2 solution for 4 h, an approximate decrease of 10 nm was noted. This indicated that the enzyme-sensitive polypeptide PVGLIG present in PVGLIG-MTX-D/T-NMs exhibited sensitivity towards MMP-2, consequently inducing a transition from stable to unstable nano-micelles with the aim of maintaining drug stability in blood while enabling rapid release in tumor cells. These findings align with those obtained from in vitro release studies conducted on nano-micelle drugs (Figure 1O and P).

Synergies or antagonisms that result in the production of multiple drugs at the tumor site typically rely on the molar ratio of the combined drugs. Therefore, selecting an appropriate ratio of synergistic drugs for in vitro and in vivo delivery plays a pivotal role in transitioning experimental drug combinations to clinical combination chemotherapy. Figure 2A and B depict two-dimensional (2D) and three-dimensional (3D) synergies resulting from the combination of free DTX and free TPL, with red area gradients indicating synergy strength. With a ZIP Synergy score of 14.758, these two drugs exhibited a high level of synergism in inhibiting SK-OV-3 cell proliferation. The concentration in the white rectangle in Figure 2A corresponds to the concentration exhibiting the highest synergistic effect, observed at DTX concentrations between 1 and 4 mm and TPL concentrations between 6.25 and 25 nM. Considering both the recommended range of drug concentrations by SynergyFinder and nano-micelle encapsulation capacity, a molar ratio of 200:1 was selected for DTX and TPL for subsequent experiments.

The results of the cytotoxicity assay are presented in Figure 2C, where it can be observed that blank micelle sets did not exert a significant impact on cell survival. This suggests that the polymer material itself possesses low toxicity and holds potential as a safe nano-material carrier. Furthermore, the cytotoxicity of other drug-carrying micelles exhibited an increase with escalating drug concentrations, indicating a time- and dose-dependent effect. Notably, MTX-D/T-NMs and PVGLIG-MTX-D/T-NMs+MMP2 demonstrated more remarkable inhibitory effects on SK-OV-3 cells at equivalent drug concentrations. This enhanced efficacy could be attributed to MTX's ability to enhance cellular uptake of MTX-D/T-NMs through folate receptor-mediated endocytosis on the surface of SK-OV-3 cells. Additionally, PVGLIG-MTX-D/T-NMs exhibited MMP-2 responsiveness under MMP2 enzyme induction, leading to hydration layer shedding and exposure of the MTX-targeting ligand. Consequently, greater intracellular drug release occurs. The half-maximal inhibitory concentration (IC_{50}) values for different nano-micelles were calculated using GraphPad Prism 9.0 software (GraphPad Prism Software Inc., San Jose, CA, USA) (Figure 2D). As depicted in Figure 2D, the IC_{50} value for PVGLIG-MTX-D/T-NMs +MMP250 was determined to be (1.74±0.119) μM, while DTX-NMs exhibited an IC_{50} value of (3.51±0.69) μM. Consistent with cytotoxicity assay, the staining results for live and dead cells supported these findings (Figure 2E and F).

The hemolysis rate is a crucial parameter utilized for characterizing blood compatibility, serving as a pivotal factor in the application of drug preparations in the human body and enabling assessment of drug toxicity levels. The hemolysis of PVGLIG-MTX-D/T-NMs at different concentrations is illustrated in Figure 2G. The findings demonstrated that the concentration-dependent hemolysis rate of PVGLIG-MTX-D/T-NMs remained below the accepted threshold of 5% in the designated concentration range (Figure 2H), indicating excellent blood compatibility and safety profiles for PVGLIG-MTX-D/T-NMs.

Receptor-mediated active targeted drug delivery systems have emerged as a prominent research area in pharmaceutics in recent years. Folate receptor alpha (FRα) is a cell surface membrane protein responsible for receiving signals from folate or folate-like substances and facilitating their entry into the cell. The expression levels of folate receptors may increase in tumor cells due to their rapid growth and high metabolic activity, necessitating higher folic acid uptake for sustained proliferation. Consequently, tumor cells upregulate the expression levels of folate receptors to meet their heightened demand for folic acid.[29] Exploiting the heightened expression of folic acid receptor on tumor cell surfaces, targeted drugs or therapeutic strategies can be devised, such as conjugating drugs with folic acid or folate-like compounds and utilizing the folic acid receptor-mediated uptake pathway for intracellular drug delivery.[30] This approach aims to enhance drug targeting and efficacy while minimizing harm to normal cells. Surface-modified MTX (MTX-Cou-NMs), a representative folate derivative, competes for binding with folate receptors present on tumor cell surfaces. To

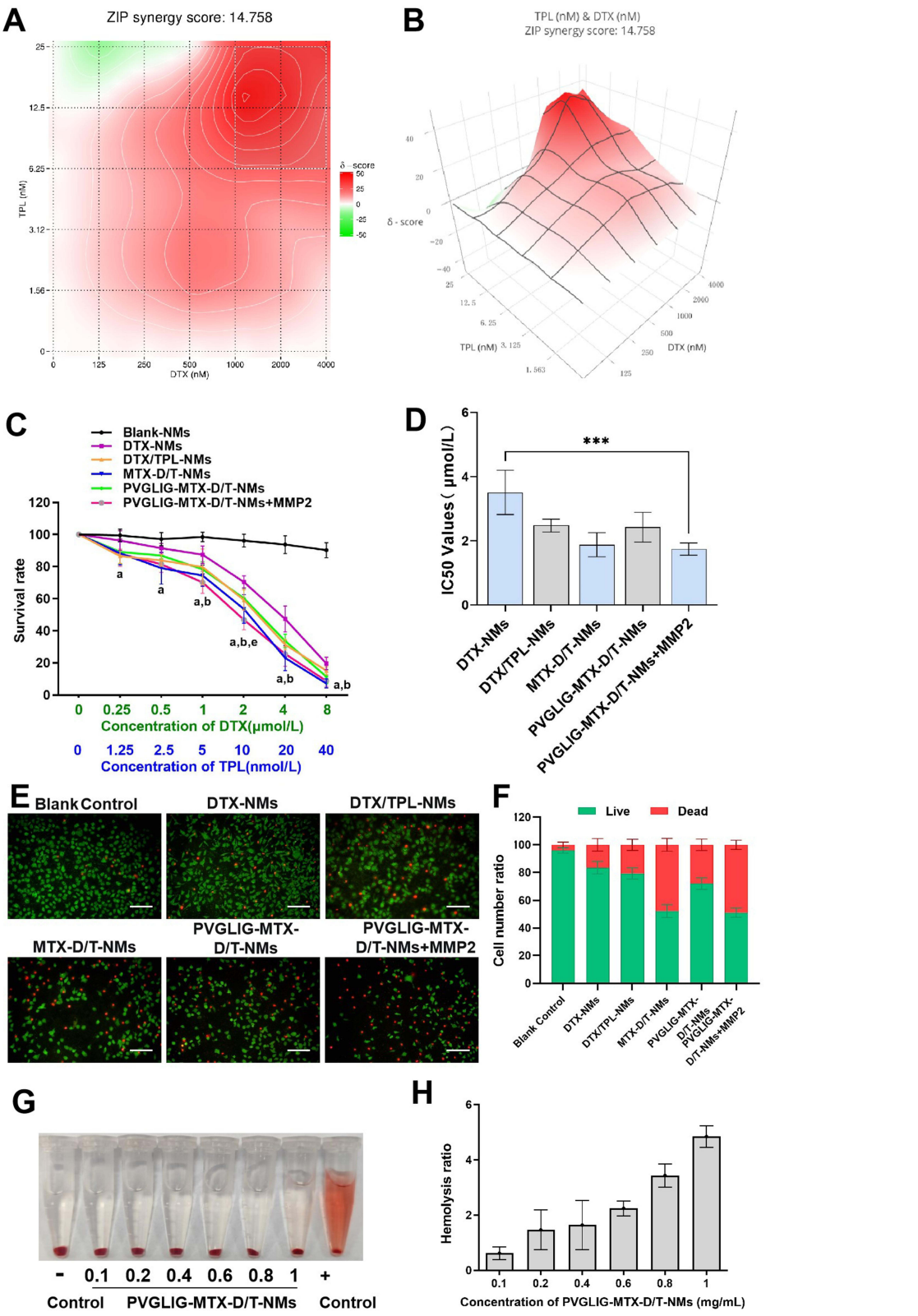

Figure 2 Analysis of cytotoxicity and in vitro hemolysis rate of SK-OV-3 cells by different drug groups. (**A**) Evaluation of the Synergistic Pharmacological Effects of Free DTX and Free TPL, 2D synergistic maps and comprehensive synergistic scores; (**B**) 3D synergies and synergies scores for the combination of free DTX and free TPL. The 2D and 3D synergy maps highlight synergistic and antagonistic dose regions in red and green colors, respectively. (**C**) Inhibition curves of SK-OV-3 cell survival rate by different micelles. (**D**) IC_{50} values of inhibitory effects of different micelles on SK-OV-3 cells. (**E** and **F**) The fluorescent staining images and statistical results of live and dead SK-OV-3 cells after treatment with different micelles. (**G** and **H**) Hemolysis of PVGLIG-MTX-D/T-NMs at different concentrations (0.1, 0.2, 0.4, 0.6, 0.8, 1 mg/mL). a, b, and e all indicated that PVGLIG-MTX-D/T-NMs +MMP2 was significantly different from other drug groups, a vs Blank-NMs, b vs DTX-NMs, e vs PVGLIG-MTX-D/T-NMs. Data to mean ± SD (n = 4), *** P <0.001.

https://doi.org/10.2147/IJN.S470219

investigate folate receptor-mediated endocytosis, the expression levels of folate receptors in SK-OV-3 cells were determined, and the intracellular nano-micelles' co-localization was assessed using laser confocal microscopy. As illustrated in Figure 3, the nucleus was visualized by blue fluorescence, each group of micelles was represented by green fluorescence, and folate receptors labeled with immunofluorescence were indicated by red fluorescence. As depicted in Figure 3, the widespread distribution of red fluorescence in the cells could be indicative of substantial expression levels of folic acid receptors on SK-OV-3 cell surfaces, aligning with previously reported outcomes. Notably, endocytosis of MTX-Cou-NMs by SK-OV-3 cells exhibited significantly higher intensity compared with Cou-NMs alone. Furthermore, a high degree of co-localization was found between the red fluorescence from folate receptors and the green fluorescence from MTX-Cou-NMs, indicating specific binding and active uptake mediated by the MTX-folate receptor interaction. Addition of folate receptor binding inhibitor (FA) to the MTX-Cou-NMs group resulted in a significant reduction in green fluorescence intensity, further supporting this conclusion.

Effective internalization of nano-particles by tumor cells and controlled release of drugs in the cells are essential prerequisites for efficient tumor inhibition. Fluorescence microscopy was employed to visualize the intensity and distribution of intracellular fluorescence. As depicted in Figure 4, the fluorescence intensity of SK-OV-3 cells in each drug administration group exhibited a time- and dose-dependent increase, indicating their uptake behavior. Notably, both

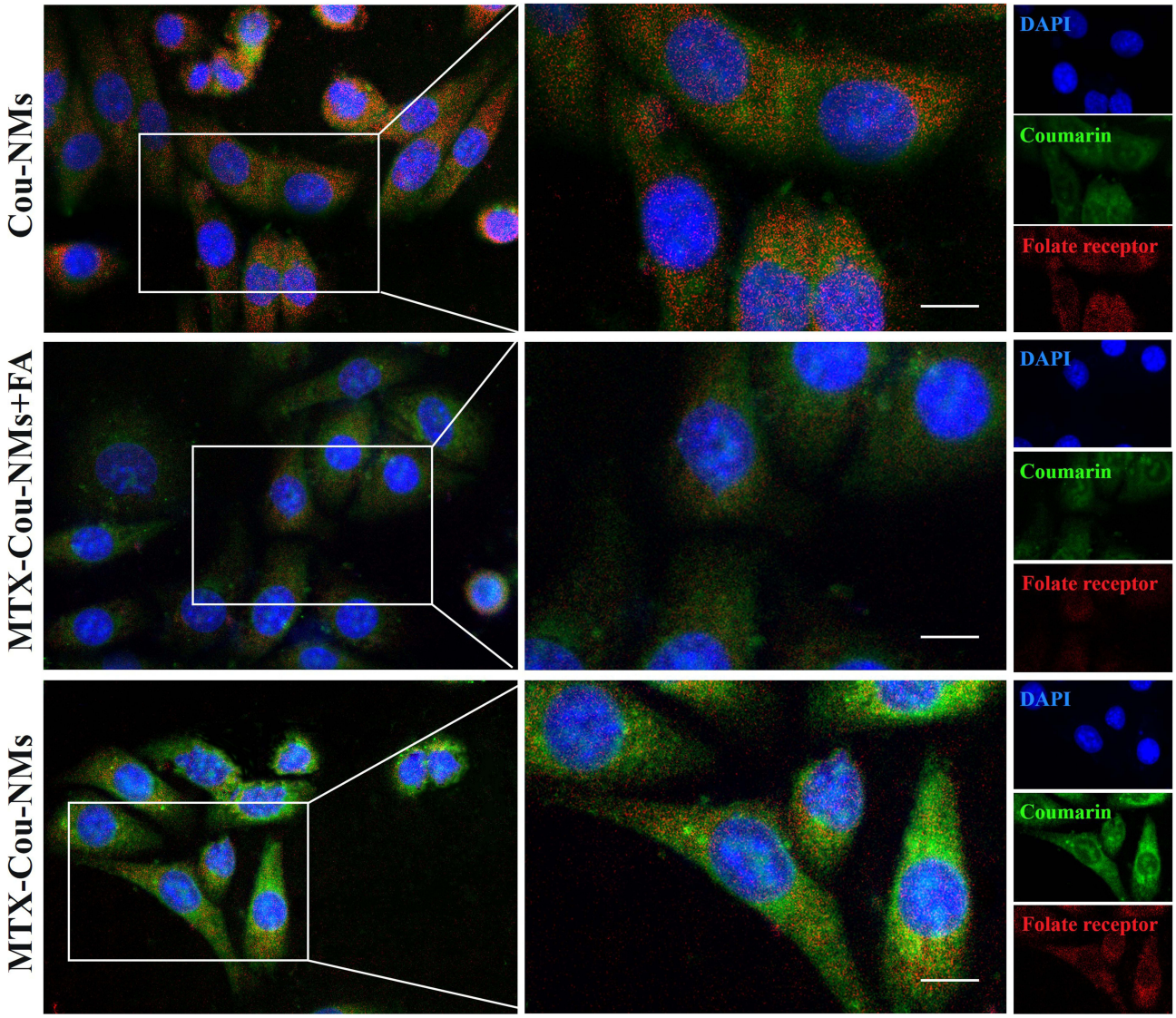

Figure 3 Expression of folate receptor on SK-OV-3 cell surface and colocalization of intracellular nanomicelles. Scale, 20μm.

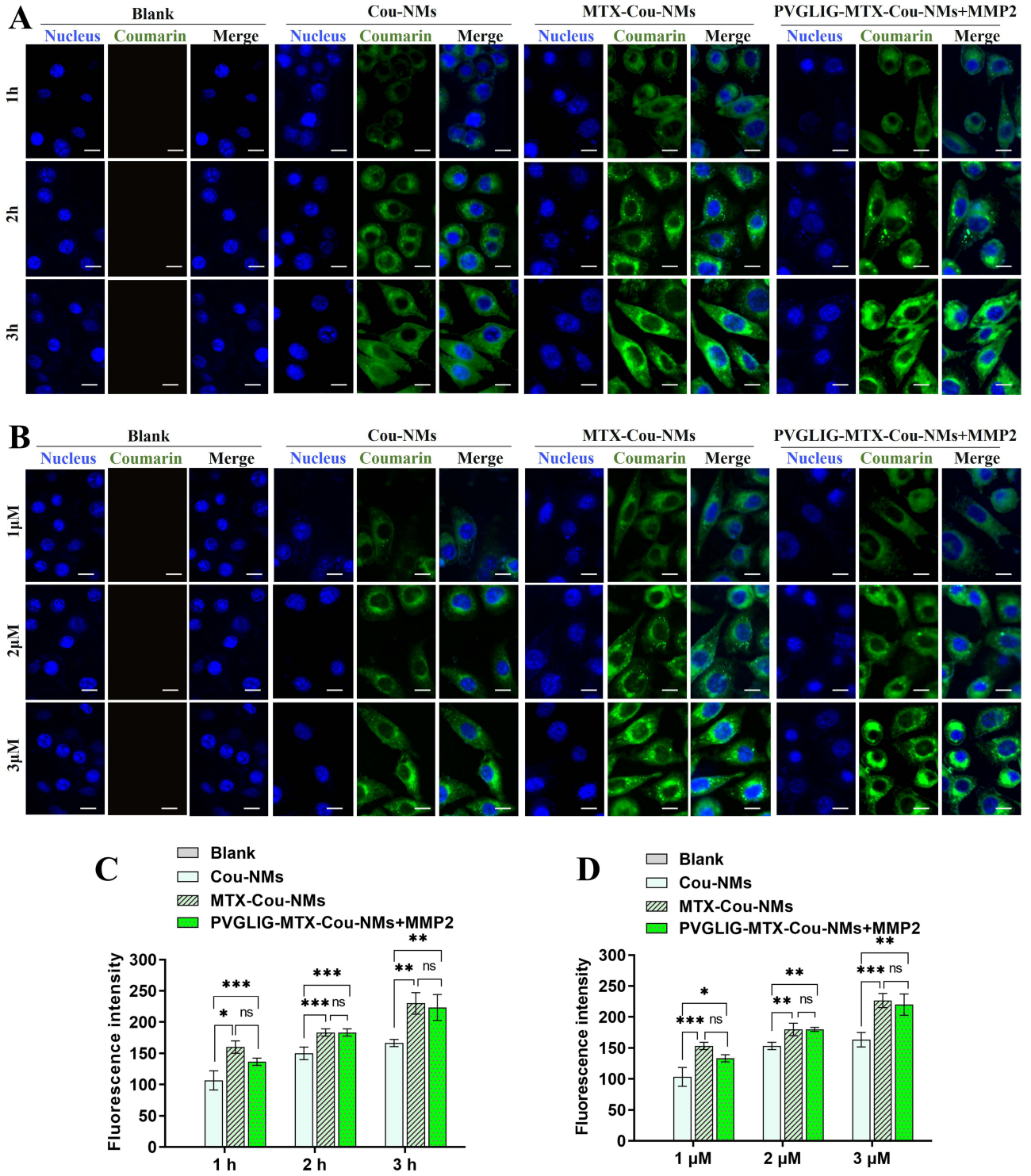

Figure 4 Qualitative analysis of the uptake of different micelles in SK-OV-3 cells by confocal laser scanning microscopy. (**A**) Uptake of different micelles in SK-OV-3 cells by confocal laser scanning microscopy and (**C**) statistical diagram; (**B**) Uptake of different micelles by SK-OV-3 cells with concentration changes and (**D**) statistical maps; Scale, 20μm. Data to mean ± SD (n = 3), the ns: **P*<0.05, ** *P* <0.01, *** *P* <0.001.

MTX-COU-NMS and PVGLIG-MTX-Cou-NMs+MMP2 groups displayed significantly higher fluorescence intensity compared with the Cou-NMs group, suggesting that MTX-modified nano-micelles facilitated rapid drug uptake by SK-OV-3 cells and enhanced their cytotoxic effect on tumor cells. These findings were further supported quantitatively through flow cytometry analysis (Figure 5).

https://doi.org/10.2147/IJN.S470219

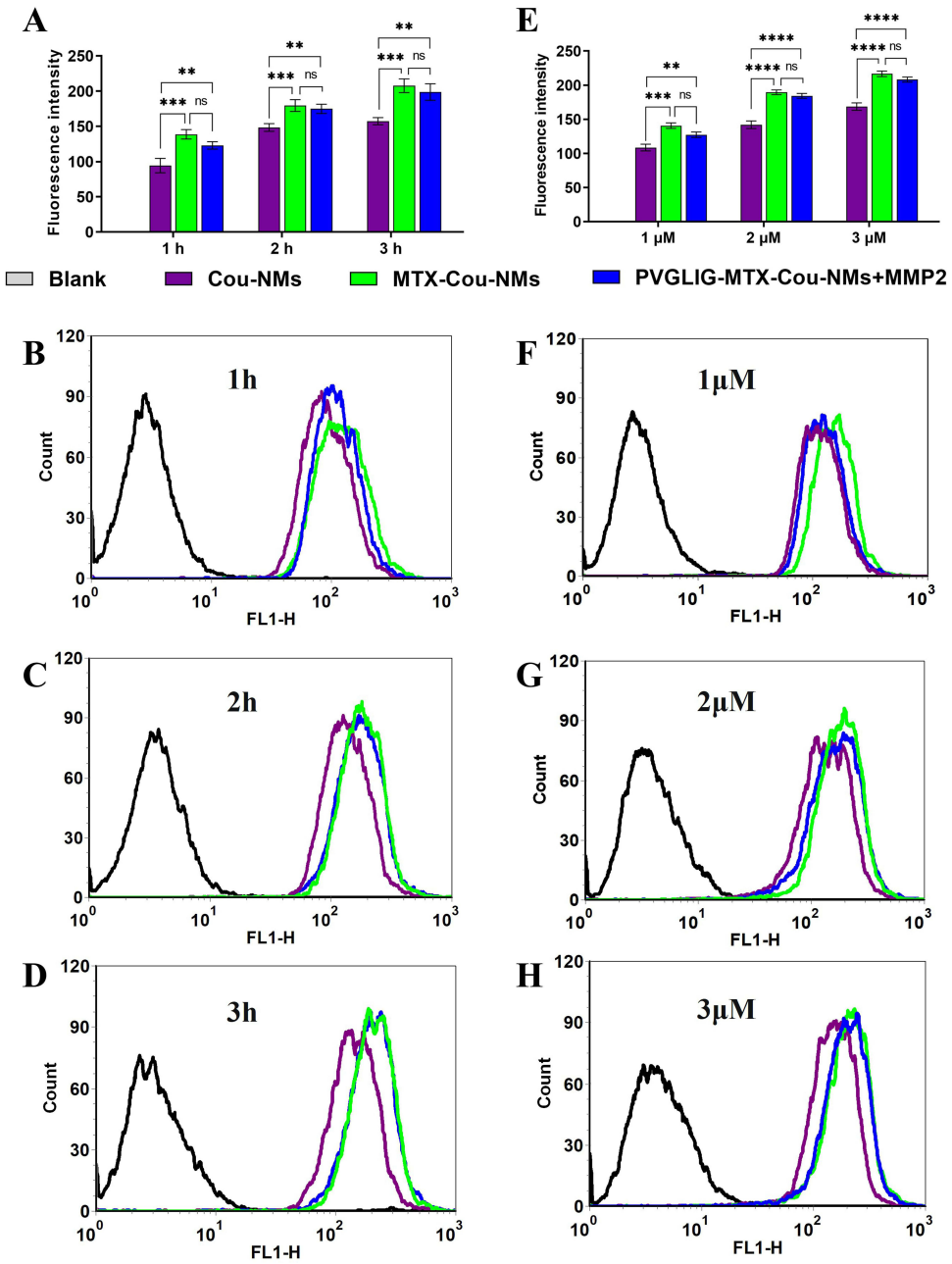

Figure 5 Quantitative analysis of the uptake of different micelles in SK-OV-3 cells by flow cytometry. (**A–D**) Uptake of different micelles in SK-OV-3 cells by flow cytometry over time; (**E–H**) Uptake of different micelles by SK-OV-3 cells with changing concentration; Scale, 20μm. Data to mean ± SD (n = 3), the ns: *P*>0.05, ** *P* <0.01, *** *P* <0.001, **** *P* <0.0001.

Malignant tumors are characterized by uncontrolled cellular proliferation and growth. The EDU kit was employed to investigate the inhibition of SK-OV-3 cell proliferation in each experimental group. As illustrated in Figure 6A and B, the blank control group exhibited a cell proliferation rate exceeding 70%, whereas all drug administration groups displayed a decrease in cell proliferation. Notably, MTX-D/T-NMs and PVGLIG-MTX-D/T-NMs+MMP2 groups demonstrated the most remarkable inhibitory effect, reducing the cell proliferation rate to approximately 20%. These results significantly differed from those of DTX-NMs treatment, indicating that TPL could synergistically enhance DTX's ability to inhibit cell proliferation.

The mechanism by which anti-tumor drugs induce apoptosis in tumor cells is through the activation of apoptotic pathways. To assess the apoptotic potential of different nano-micelles, Hoechst 33342 apoptosis staining and Annexin-

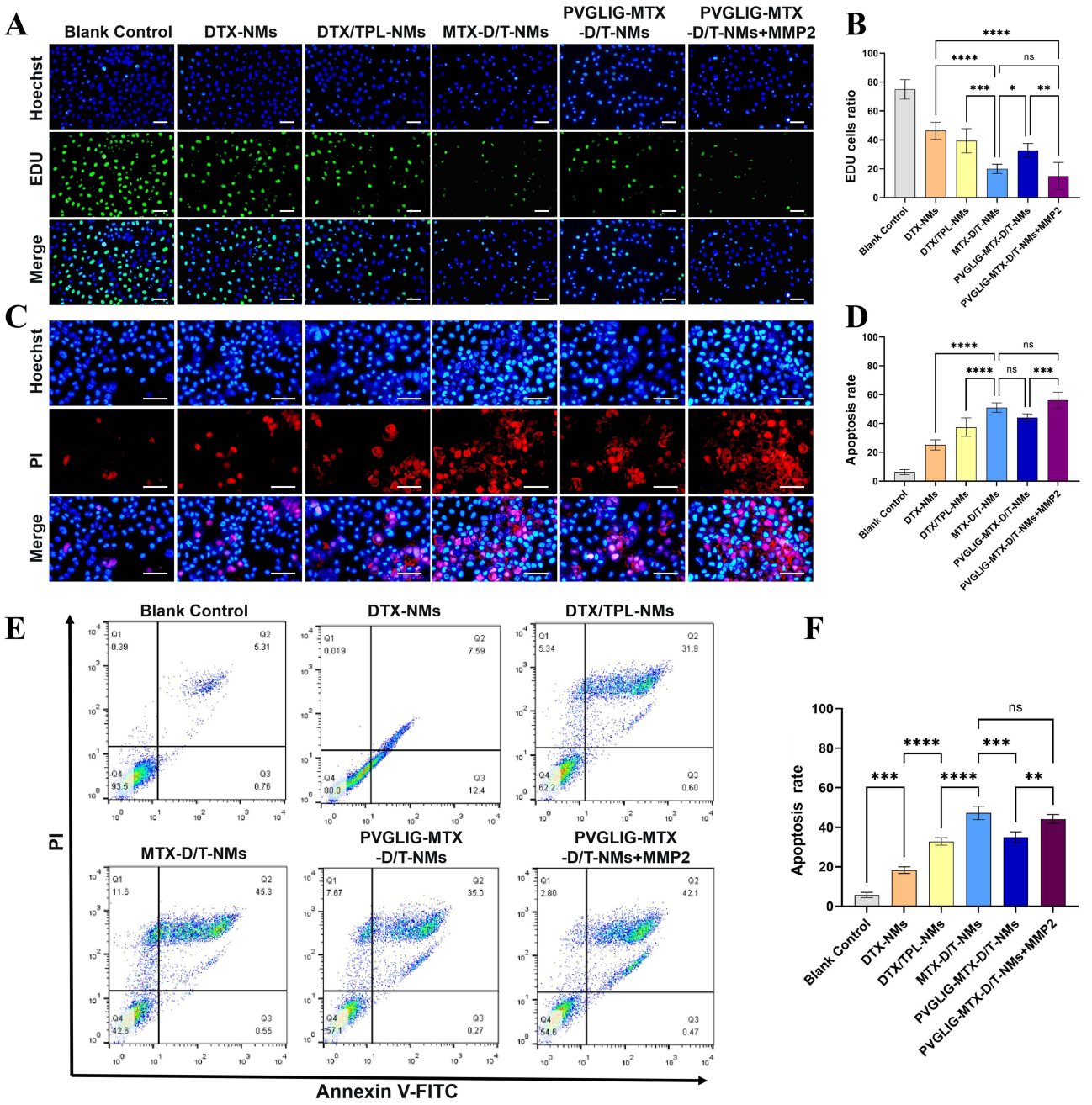

Figure 6 Multiplication and apoptosis analysis of SK-OV-3 cells after treatment with different nanomicelles. (**A**) EDU proliferation analysis of SK-OV-3 cells; (**B**) cell proliferation rate; (**C**) Hoechst 33342/PI double staining was used to detect the effect of nanometer micelles on cell apoptosis in each group; (**D**) Apoptosis results of Hoechst 33342/PI double staining; (**E**) Apoptosis was detected by flow cytometry; (**F**) quantitative analysis of apoptotic index. Scale, 100μm. Data to mean±SD (n = 3), the ns: *P*>0.05, **P*<0.05, ** *P* <0.01, *** *P* <0.001, **** *P* <0.0001.

FITC and propidium iodide (PI) double staining were performed. Hoechst 33342, a blue fluorescent DNA dye, effectively permeates the cell membrane and stains the nucleus blue, enabling quantification of total cell count.[31] On the other hand, PI selectively stains apoptotic cells with weak red fluorescence and dead cells with strong red fluorescence as it does not penetrate intact cell membranes. As displayed in Figure 6C and D, all drug administration groups exhibited higher levels of red fluorescence compared with the blank control group, indicating successful induction of apoptosis in SK-OV-3 cells across all treatment conditions. Notably, MTX-D/T-NMs and PVGLIG-MTX-D/T-NMs +MMP2 groups displayed a greater number of nuclei with high fluorescence intensity indicative of extensive apoptosis induction capacity. The distinction between DTX-NMS group and DTX/ TPL-NMS group confirmed that TPL

https://doi.org/10.2147/IJN.S470219

synergistically enhanced DTX-induced apoptosis. Furthermore, the disparity between DTX/TPL-NMs group and MTX-D/T-NMs group could be attributed to the enhanced cellular uptake mediated by specific binding between MTX-D/T-NMs and folate receptors via endocytosis mechanisms. Importantly, PVGLIG-MTX-D/T-NMs+MMP2 group demonstrated comparable apoptotic ratios to MTX-D/T-NMs group while significantly surpassing PVGLIG-MTX-D/T-NMs group due to MMP-2 sensitive peptide cleavage under MMP2 enzyme action, resulting in shedding of dense PEG_{5000} hydration layer, thereby exposing more MTX for improving drug internalization by tumor cells.

The results of AnnexinV-FITC flow cytometry analysis on apoptosis of SK-OV-3 cells induced by nano-micelles were consistent with the findings from Hoechst 33342/PI apoptosis staining (Figure 6E). The flow cytometry is based on the principle that Annexin-FITC can specifically bind to phosphatidylserine exposed on the cell membrane during early stages of apoptosis, while PI can stain the nucleus through the compromised membranes of late apoptotic and dead cells. This method enables detection of both early and late apoptotic cells. Flow cytometry was employed to quantitatively assess the rates of early and late apoptotic as well as necrotic SK-OV-3 cells, which were subsequently compared among different treatment groups. As depicted in Figure 6F, in the blank control group, only 6.07% exhibited total apoptosis rate (early + late). The descending order for total apoptosis rate in each treatment group was as follows: DTX-NMs<DTX/TPL-NMs≈PVGLIG-MTX-D/T-NMs<MTX-D/T-NMs≈PVGLIG-MTX-D/T-NMs+MMP2.

The wound healing assay is a widely employed method for assessing the migratory and invasive capabilities of cells. This involves creating scratches on cell culture dishes and observing the extent to which these scratches are filled by cells over a specific time period. After 24 h of treatment, the scratches in the blank control group exhibited substantial healing (Figure 7A and E), while the administration group showed varying degrees of inhibition in scratch closure, and MTX-D/T-NMs and PVGLIG-MTX-D/T-NMs+MMP2 groups demonstrated the most remarkable inhibitory effects.

The inhibitory effects of different micelle groups on the invasion and migration of SK-OV-3 cells were evaluated using the Transwell assay. Representative images of cells in each group after passing through the Transwell chamber following treatment with different micelles are illustrated in Figure 7B and C. Figure 7B and F represent the results of cell migration inhibition, while Figure 7C and G represent the results of cell invasion inhibition. In both experiments, a substantial number of cells from the blank control group passed through the Transwell chamber, indicating strong migration and invasion capabilities of SK-OV-3 cells. Compared with the blank control group, all drug administration groups exhibited a decrease in the number of cells passing through the Transwell chamber; among them, MTX-D/T-NMs and PVGLIG-MTX-D/T-NMs+MMP2 exhibited significant inhibitory effects on cell migration and invasion, and both rates decreased to less than 10%.

Malignant tumor cells possess the ability to undergo deformation and degrade the basement membrane, facilitating their interconnection into mesh-like structures known as VM. This phenomenon enables tumor cells to acquire oxygen and nutrients, thereby promoting tumor growth and metastasis. In the field of tumor biology, antigenic mimicry is considered as a significant phenomenon associated with tumor angiogenesis that can impact tumor growth, invasion, and metastasis.[32] Figure 7D and H illustrate the disruptive effects of different micelles on VM channels. In the blank control group, well-defined channels composed of elongated cells were observed with a complete mesh structure and large mesh area. However, VM channels formed by SK-OV-3 cells exhibited varying degrees of damage after exposure to different micellar groups. MTX-D/T-NMs and PVGLIG-MTX-D/T-NMs+MMP2 groups demonstrated notable inhibition in VM channel formation due to shortened or fragmented channels with poor mesh integrity or absence of mesh formation, altogether resulting in smaller individual mesh areas.

The PVGLIG-MTX-D/T-NMs developed in this study exhibited favorable targeted cellular uptake in vitro. To investigate their targeting efficacy at the animal level in vivo, in vivo targeting experiments were conducted. Figure 8 illustrates the distribution of each preparation group in tumor-bearing nude mice. It was revealed that the fluorescence intensity at the tumor site was significantly stronger in each micelle group compared with the free DiR group. Moreover, within 12 h, the fluorescence signal at the tumor site was enhanced over time and remained detectable up to 72 h in vivo. In contrast, DiR from the free group mainly accumulated in the liver, exhibiting a very weak fluorescence signal at the tumor site, which disappeared after 48 h in vivo. Among all micelle groups tested, PVGLIG-MTX-D/T-NMs group demonstrated prolonged half-life due to their PEG_{5000} hydration film coating on nano-micelles' outermost layer that facilitated long circulation and enhanced stability during blood circulation. Additionally, both MTX-modified nano-

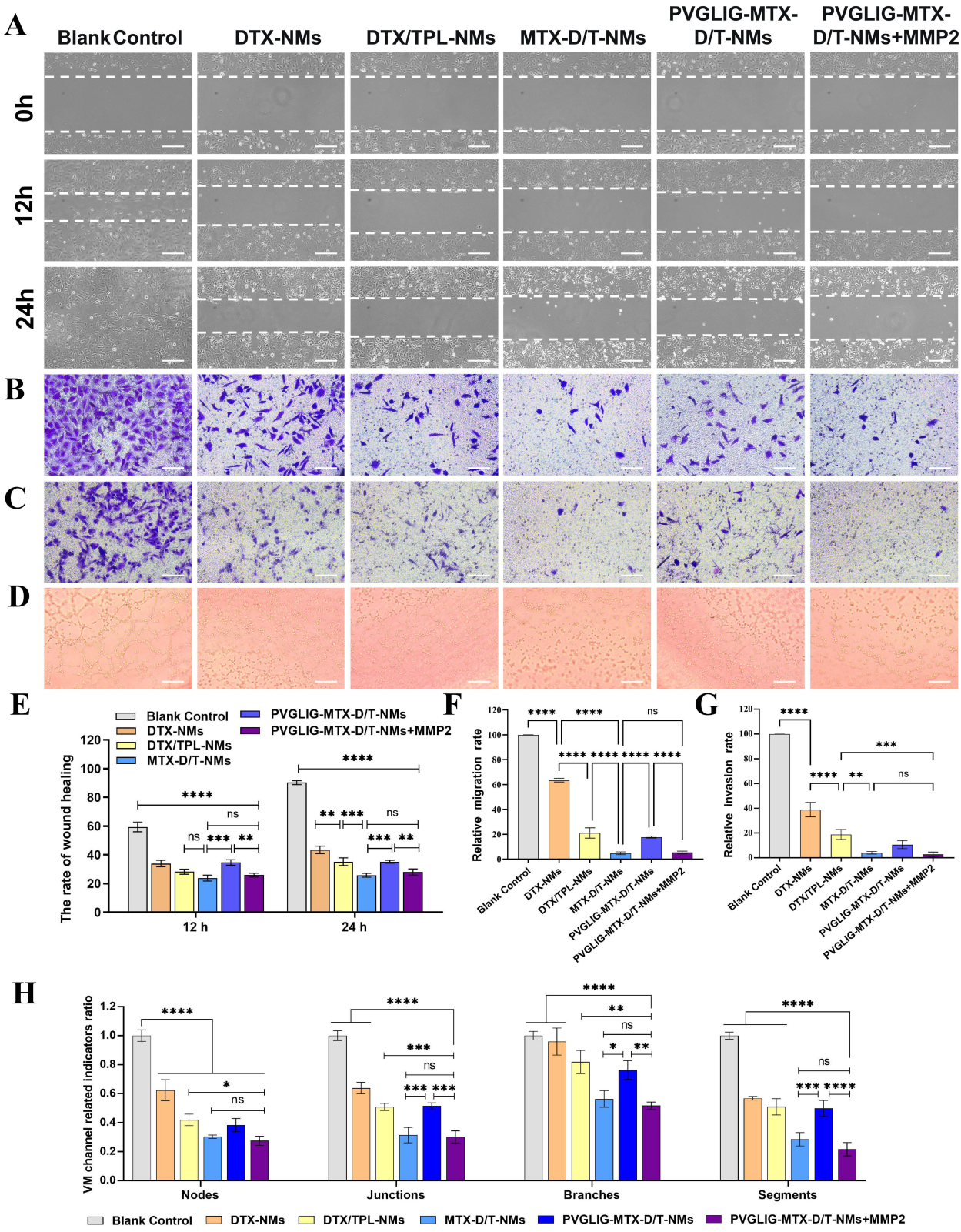

Figure 7 Inhibitory effects of nano-micelles on invasion, migration and VM channel of SK-OV-3 cells (**A**) Images of wound healing; (**B**) images of migration of SK-OV-3 cells; (**C**) images of invasion of SK-OV-3 cells; (**D**) images of inhibited VM channel formation; (**E**) quantitative analysis of wound healing rates; (**F**) semi-quantitative analysis of mobility; (**G**) semi-quantitative analysis of invasion rate; (**H**) semi-quantitative analysis of VM channel related indicators. Scale, 100μm. Data to mean±SD (n = 3), the ns: $P>0.05$, *$P<0.05$, ** $P<0.01$, *** $P<0.001$, **** $P<0.0001$.

https://doi.org/10.2147/IJN.S470219

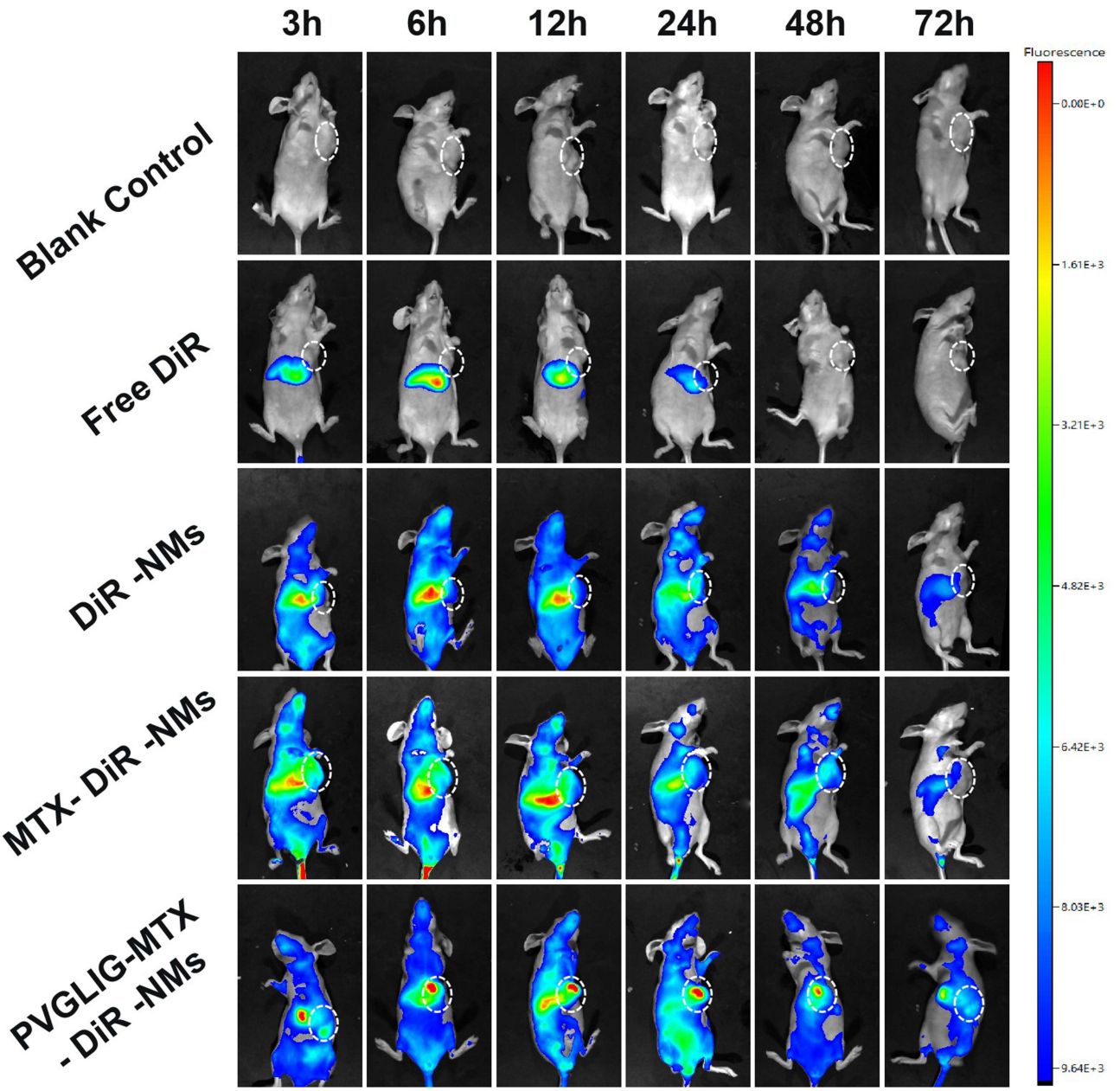

Figure 8 Distribution of different nanomicelles in tumor-bearing nude mice.

micelle groups successfully delivered fluorescent signals to tumor lesions of nude mice, indicating active targeting ability and higher accumulation level at tumor sites as conferred by MTX modification. These findings confirmed both stability and active targeting capability of PVGLIG-MTX-D/T-NMs during blood circulation and paved an experimental basis for future in vivo targeted therapy using these nano-drugs.

In vivo experiments were conducted, as displayed in Figure 9A. Considering the potent therapeutic effects of DTX and TPL on cancer cells, alongside their associated serious adverse reactions, in vivo experiments were carried out to partially evaluate the biosafety of PVGLIG-MTX-D/T-NMs. To assess systemic safety, the body weight of mice in each group was monitored throughout the treatment period, H&E staining was performed on normal tissues, and blood samples were collected from the orbital sinus to evaluate liver function.

The weight of tumor-bearing nude mice in the free DTX/TPL group decreased, while the control group exhibited weight gain due to uncontrolled tumor growth (Figure 9B). Weight loss in the free DTX/TPL group was likely attributed

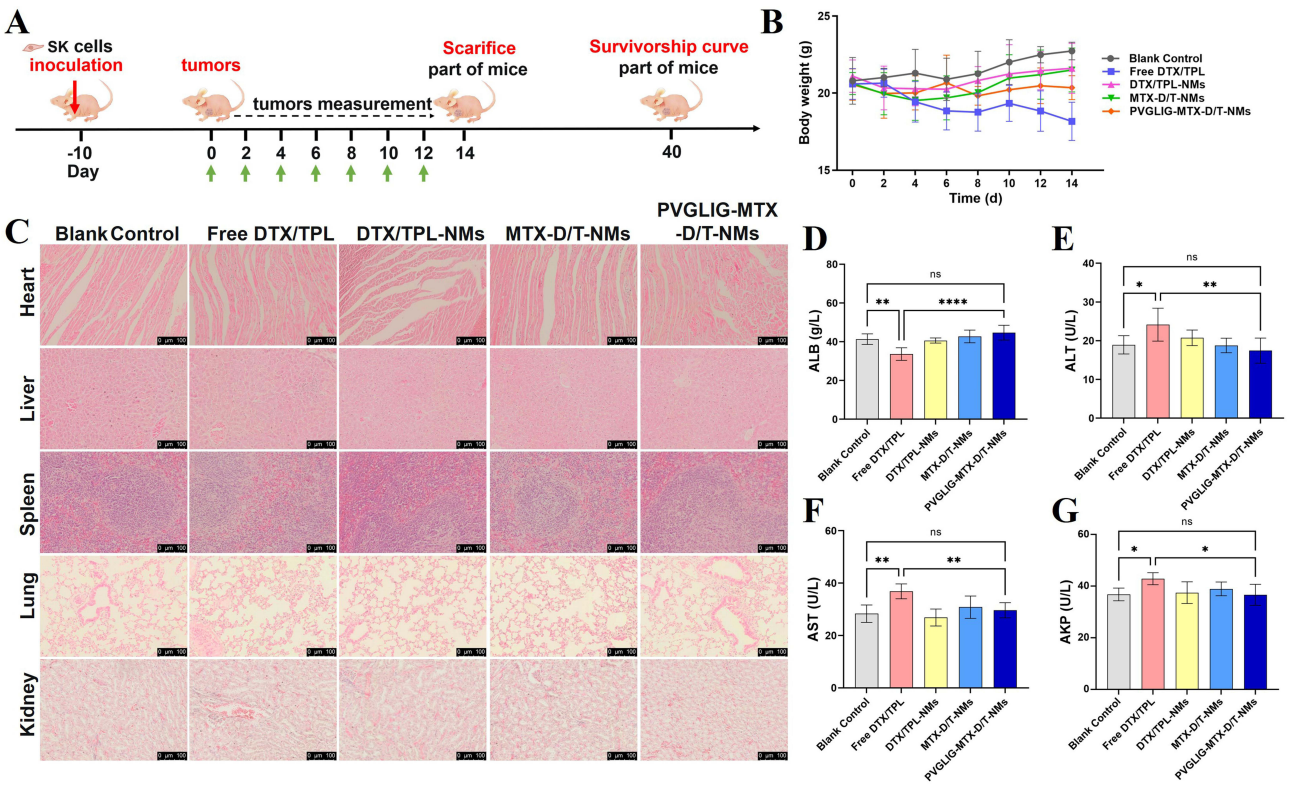

Figure 9 Therapeutic regimen and in vivo safety evaluation of tumor-bearing nude mice. (**A**) Schedule of experiments in nude mice; (**B**) body weight changes of tumor-bearing nude mice after different preparations; (**C**) H&E staining map of major organs; Biochemical analysis results of (**D**) ALB, (**E**) ALT, (**F**) AST, (**G**) AKP. Scale bar: 100 μm. The ns: $P>0.05$, *$P<0.05$, ** $P<0.01$, **** $P<0.0001$.

to systemic toxicity caused by the free drug. Conversely, no significant changes in body weight were noted in other micelle groups, indicating that drug encapsulation in the micelles could effectively mitigate toxic side effects associated with DTX and TPL administration. H&E staining results (Figure 9C) revealed inflammatory cell infiltration in the liver in the free DTX/TPL group, along with dilated and hyperemic interstitial blood vessels accompanied by inflammatory cell infiltration in the kidney. These findings suggested that administration of free drugs could induce liver and kidney damage, aligning with our observations of weight loss among nude mice receiving this treatment regimen. Negligible H&E staining results were obtained for each micelle group and for the blank control group.

The liver function can be evaluated by measuring the levels of albumin (ALB), alanine aminotransferase (ALT), aspartate aminotransferase (AST), and alkaline phosphatase (AKP) in the bloodstream.[33] As ALB is primarily synthesized by the liver, hepatic damage may lead to reduced ALB synthesis, resulting in decreased serum ALB level. ALT and AST are enzymes predominantly present in hepatocytes, while AKP is mainly found in the liver and biliary system. When liver cells are damaged, these enzymes are released into the bloodstream, leading to the elevated serum levels of ALT, AST, and AKP. In comparison with other treatment groups, the free DTX/TPL group exhibited a decrease in ALB level, whereas an increase in ALT, AST, and AKP levels (Figure 9D–G). This suggests that the free DTX/TPL group could potentially impair liver function. Conversely, parameters observed in the nano-micelle group were closely comparable to those of the blank control group. These findings demonstrated its high efficiency and low toxicity advantages, which might be attributed to its strong tumor targeting ability and limited distribution in normal tissues.

The therapeutic effects of each preparation group on ovarian cancer-bearing nude mice are illustrated in Figure 10. According to the survival analysis of tumor-containing mice (Figure 10A), all mice in the blank control group and the free DTX/TPL group succumbed within 24 and 28 days, respectively, while various nano-micelle groups exhibited an extended lifespan for mice, in which PVGLIG-MTX-D/T-NMs group demonstrated the longest survival time. The tumor volume in the blank control group was significantly larger than that in the PVGLIG-MTX-D/T-NMs group, which

https://doi.org/10.2147/IJN.S470219

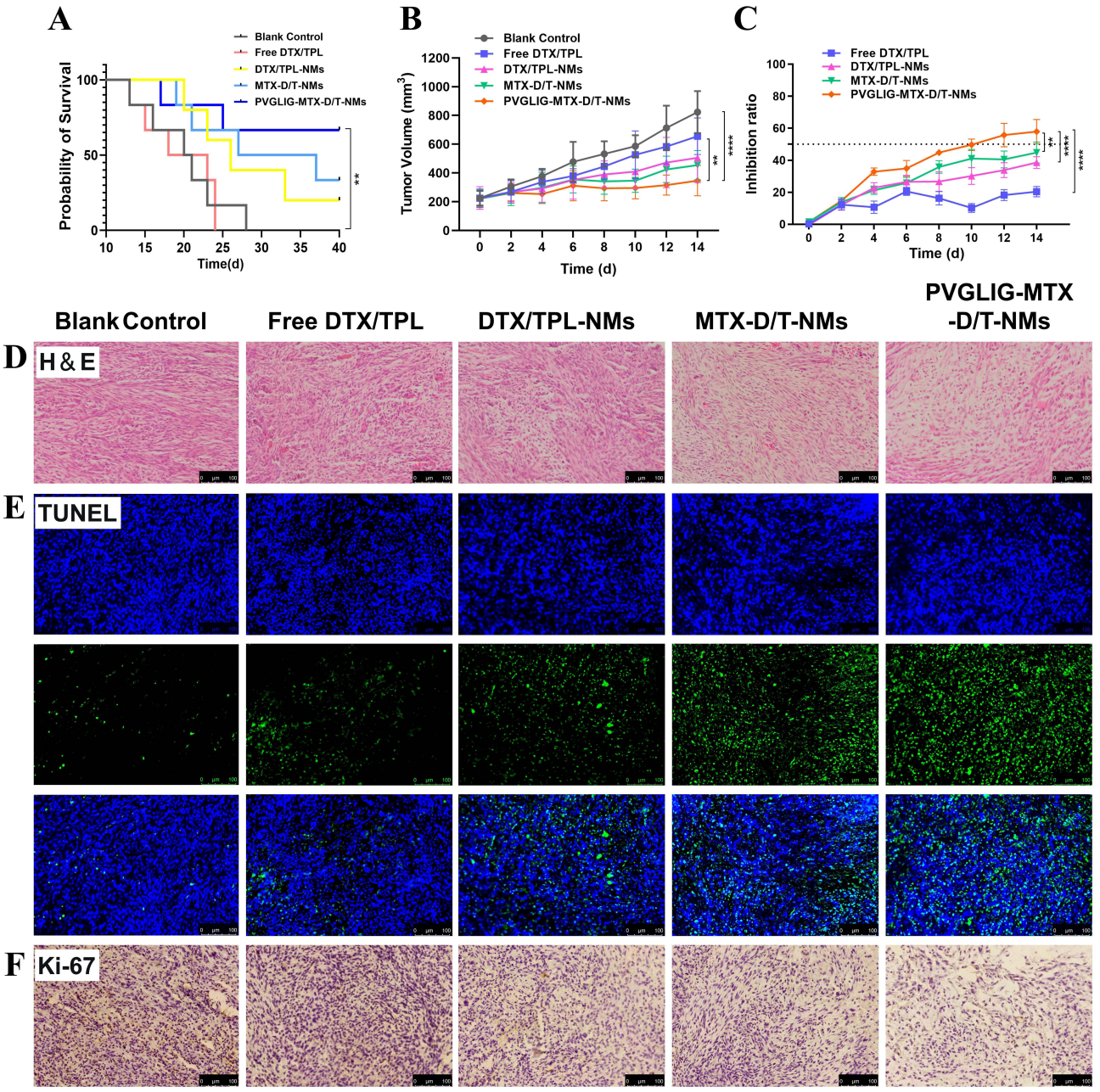

Figure 10 Therapeutic effects of each group of preparations on nude mice bearing ovarian cancer. (**A**) Comparison of survival time of tumor-bearing mice after different preparations; (**B**) the change curve of tumor volume; (**C**) tumor inhibition rate; (**D**) H&E staining images of tumor tissue sections; (**E**) TUNEL staining, positive staining indicates apoptosis; And (**F**) immunohistochemical staining of Ki-67 in tumor tissue. Scale, 100 μm. Data to mean±SD (n = 6), ** ***P*** <0.01, **** ***P*** <0.0001.

displayed a smaller tumor volume along with a statistically significant tumor inhibition rate exceeding 50% (P<0.05) (Figure 10B–C). These findings indicated that PVGLIG-MTX-D/T-NMs could effectively enhance the therapeutic efficacy of DTX and TPL against ovarian cancer. H&E staining results from tumor tissue sections are presented in Figure 10D. In the blank control group, tumor cells were densely arranged with a complete internal matrix structure. Various degrees of apoptotic morphological characteristics were observed across different nano-micelle groups, leading to a significant reduction in tumor cell density, accompanied by cytoplasmic disappearance and vacuolation occurrence. Notably, PVGLIG-MTX-D/T-NMs demonstrated the most noticeable apoptosis among all groups studied, further validating their superior anti-tumor effects.

TUNEL staining can be utilized for assessing tumor cell apoptosis in tissue sections. The principle of TUNEL staining involves using Terminal deoxynucleotidyl transferase (TdT) to label DNA break sites by attaching dUTP at the broken end of DNA, followed by marking these sites with fluorescence or stain to form visible signals.[34] By examining the staining results, it is feasible to determine whether cells can undergo apoptosis. Ki-67 is a nuclear protein antigen that is mainly used for the pathological diagnosis and prognosis assessment of tumor tissue. Generally, higher positive rates of Ki-67 indicate stronger proliferative activity of tumor cells and potentially higher malignancy levels.[35] The results of the TUNEL staining in the PVGLIG-MTX-D/T-NMs group (Figure 10E) exhibited the greenest fluorescence, while Ki-67 immunohistochemistry results (Figure 10F) showed significantly reduced brown areas compared with other groups. These findings suggested that PVGLIG-MTX-D/T-NMs could promote tumor cell apoptosis and inhibit proliferation in nude mice, thereby exerting an anti-ovarian cancer effect. Compared with the MTX-D/T-NMs group, the PVGLIG-MTX -D/T-NMs group demonstrated further improved tumor inhibition effects.

The invasion and metastasis of tumors are characterized by a sequential degradation of the ECM, shedding of cells, migration of cells, and neovascularization.[36] Epithelial-mesenchymal transition (EMT) is defined by the loss of cell adhesion and acquisition of migratory properties. This cytological mechanism has noticeably attracted researchers' attention as the initiating event in the cascade, leading to tumor metastasis. During tumor development, certain epithelial tumor cells can undergo EMT, resulting in loss of epithelial cell polarity and adhesion while gaining interstitial-like movement and invasive capabilities. These transformed cells can breach the basement membrane, enter blood or lymphatic vessels, and disseminate through circulation, ultimately forming distant metastatic tumors. Inhibition of EMT may hold promise for preventing tumor invasion and metastasis.[37,38]

In tumors, E-Cadherin and N-Cadherin are pivotal cell adhesion proteins associated with interepithelial junction and epithelial-stromal transition, respectively. Generally, upregulation of E-Cadherin facilitates intercellular adhesion and maintains tissue structure stability, whereas N-Cadherin is mainly linked to EMT, promoting cellular migration and invasion. Consequently, reduced expression level of E-Cadherin and the elevated expression level of N-Cadherin are frequently indicative of tumor malignancy and are correlated with the enhanced metastatic potential.[39]

Angiogenesis is a crucial component of tumor growth and metastasis, providing oxygen and nutrients to tumors, as well as pathways for tumor cells to metastasize. Anti-tumor metastasis is closely associated with anti-tumor angiogenesis.[40] Vascular endothelial growth factor (VEGF) is a crucial factor to induce angiogenesis, and it plays a pivotal role in regulating angiogenesis, maintaining vascular permeability, and promoting the growth of vascular endothelial cells.[41] Hypoxia-induced-factor-1 (HIF-1) is recognized as the main regulator of hypoxic response, which can promote the expression levels of VEGF and MMP-2, promote tumor vascularization, and enhance the invasion ability of tumor cells.[42] By transcriptional regulation of its target genes, HIF-1 can promote the adaptation of cells to hypoxia, thereby enhancing tumor angiogenesis, invasion, and metastasis. The rapid expansion of tumor cells, when the growth rate is greater than the ability of the existing vasculature to provide oxygen and nutrients, may result in oxygen deficiency in the TME, increasing the expression level of HIF-1.

According to the abovementioned background, the present study investigated the expression levels of invasion- and metastasis-associated proteins in tumor tissues of mice following treatment (Figure 11). It was revealed that TPL could synergize with DTX to increase the expression level of E-Cadherin, while reduce the expression levels of N-Cadherin, MMP-2, MMP-9, HIF-1α, and VEGFA. This inhibition led to a decrease in ECM degradation, thereby suppressing angiogenesis as well as tumor cell invasion and metastasis. Compared with the blank control group, the PVGLIG-MTX -D/T-NMs group exhibited significant variations in fluorescence signal intensity among all preparation groups, indicating its superior therapeutic effects.

Conclusion

As cancer treatment research progresses, improving chemotherapy's efficacy while minimizing side effects has emerged as a critical area of concentration, and nano-medicine delivery systems have exhibited promising potential. In this study, a nano-micelle delivery system (PVGLIG-MTX-D/T-NMs) responsive to MMP-2 was designed and developed for the dual delivery of docetaxel and triptolide for the treatment of ovarian cancer. This system utilized the EPR effect and folate receptor-mediated endocytosis to achieve both passive and active targeting of tumors. This dual targeting approach

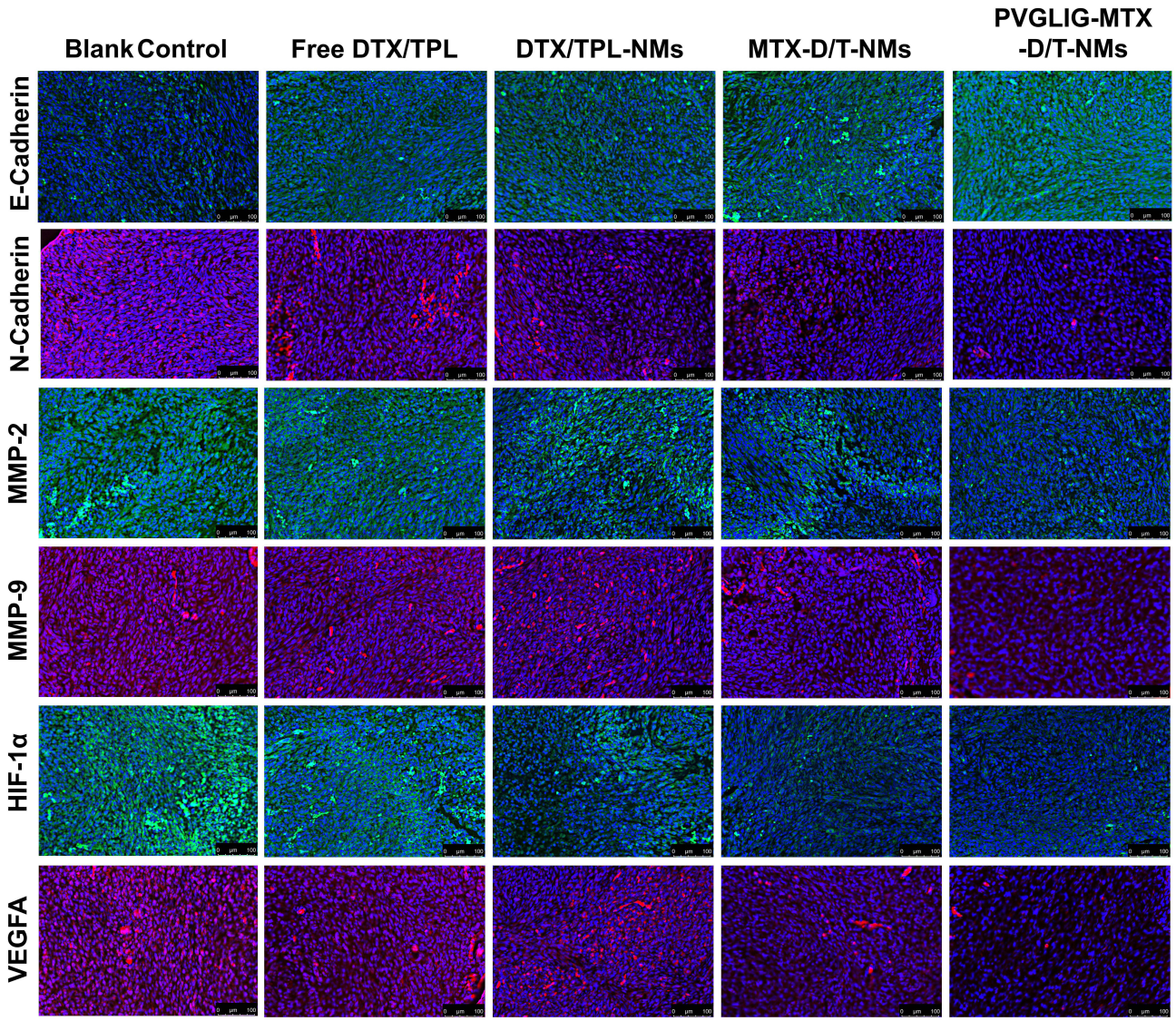

Figure 11 Immunofluorescence staining images of E-Cadherin, N-Cadherin, MMP-2, MMP-9, HIF-1α, and VEGFA in tumor tissue.

allows the nano-micelles to maintain good stability in the bloodstream, improving drug accumulation in tumor tissue and enhancing therapeutic outcomes. Compared with free drugs, nano-micelles significantly reduce drug toxicity and side effects, thereby improving treatment safety, which is an important advancement for patient compliance and tolerance. The specific ratio of docetaxel and triptolide in the nano-micelles exhibited synergistic antitumor effects, providing certain scientific evidence for combination chemotherapy in clinical practice. This system could successfully inhibit EMT and angiogenesis in ovarian cancer by regulating the expression levels of tumor-related proteins, such as E-cadherin, N-cadherin, MMPs, HIF-1α, and VEGF, thereby reducing the invasive and metastatic capabilities of the tumor. The abovementioned advantages make PVGLIG-MTX-D/T-NMs a promising candidate for targeted therapy in oncology.

Acknowledgments

This work was supported by the Open fund of Key Laboratory of Ministry of Education for TCM Viscera-State Theory and Applications, Liaoning University of Traditional Chinese Medicine [Grant No.zyzx2404, No.zyzx2301], China Postdoctoral Science Foundation [Grant No.2022MD723796], the Doctoral Start-up Foundation of Liaoning Province [Grant No.2023-BS-139], Basic Research Project of Education Department of Liaoning Province [Grant No.JYTQN

2023471], the National Natural Science Foundation of China [Grant No.82204629] and the Liaoning Province Natural Science Foundation doctoral foundation [Grant No.2022-BS-197].

Author Contributions

All authors made a significant contribution to the work reported, whether that is in the conception, study design, execution, acquisition of data, analysis and interpretation, or in all these areas; took part in drafting, revising or critically reviewing the article; gave final approval of the version to be published; have agreed on the journal to which the article has been submitted; and agree to be accountable for all aspects of the work. All authors have read and approved the final manuscript.

Funding

This work was supported by the Open fund of Key Laboratory of Ministry of Education for TCM Viscera-State Theory and Applications, Liaoning University of Traditional Chinese Medicine [Grant No.zyzx2404, No.zyzx2301], China Postdoctoral Science Foundation [Grant No.2022MD723796], the Doctoral Start-up Foundation of Liaoning Province [Grant No.2023-BS-139], Basic Research Project of Education Department of Liaoning Province [Grant No.JYTQN 2023471], the National Natural Science Foundation of China [Grant No.82204629] and the Liaoning Province Natural Science Foundation doctoral foundation [Grant No.2022-BS-197].

Disclosure

The authors report no conflicts of interest in this work.

References

1. Konstantinopoulos PA, Matulonis UA. Clinical and translational advances in ovarian cancer therapy. *Nat Cancer*. 2023;4(9):1239–1257. doi:10.1038/s43018-023-00617-9
2. Sipos A, Ujlaki G, Mikó E, et al. The role of the microbiome in ovarian cancer: mechanistic insights into oncobiosis and to bacterial metabolite signaling. *Mol Med*. 2021;27:1–20. doi:10.1186/s10020-020-00255-2
3. Dizon DS. PARP inhibitors for targeted treatment in ovarian cancer. *Lancet*. 2017;390(10106):1929–1930. doi:10.1016/S0140-6736(17)32418-2
4. Bose S, Saha P, Chatterjee B, Srivastava AK. Chemokines driven ovarian cancer progression, metastasis and chemoresistance: potential pharmacological targets for cancer therapy. In: *Seminars in Cancer Biology*. Elsevier; 2022:568–579.
5. Wang L, Wang X, Zhu X, et al. Drug resistance in ovarian cancer: from mechanism to clinical trial. *Mol Cancer*. 2024;23(1):66. doi:10.1186/s12943-024-01967-3
6. Zhang Y, Wang Y, Zhao G, Orsulic S, Matei D. Metabolic dependencies and targets in ovarian cancer. *Pharmacol Ther*. 2023;245:108413.
7. Sheng D, Ma W, Zhang R, et al. Ccl3 enhances docetaxel chemosensitivity in breast cancer by triggering proinflammatory macrophage polarization. *J ImmunTher Cancer*. 2022;10(5):e003793. doi:10.1136/jitc-2021-003793
8. Wang S, Zhou D, Xu Z, et al. Anti-tumor drug targets analysis: current insight and future prospect. *Curr Drug Targets*. 2019;20(11):1180–1202. doi:10.2174/1389450120666190402145325
9. McMullen M, Madariaga A, Lheureux S. New approaches for targeting platinum-resistant ovarian cancer. In: *Seminars in Cancer Biology*. Elsevier; 2021:167–181.
10. Xu H, Liu B. Triptolide-targeted delivery methods. *Eur J Med Chem*. 2019;164:342–351. doi:10.1016/j.ejmech.2018.12.058
11. Zhang Z, Sun C, Zhang L, et al. Triptolide interferes with XRCC1/PARP1-mediated DNA repair and confers sensitization of triple-negative breast cancer cells to cisplatin. *Biomed Pharmacother*. 2019;109:1541–1546. doi:10.1016/j.biopha.2018.11.008
12. Roett MA, Evans P. Ovarian cancer: an overview. *Am Family Phys*. 2009;80(6):609–616.
13. von Wolff M, Germeyer A, Böttcher B, et al. Evaluation of the gonadotoxicity of cancer therapies to improve counseling of patients about fertility and fertility preservation measures: protocol for a retrospective systematic data analysis and a prospective cohort study. *JMIR Res Protocols*. 2024;13(1):e51145. doi:10.2196/51145
14. Zhang T, Li M, Yang R, et al. Therapeutic efficacy of lipid emulsions of docetaxel-linoleic acid conjugate in breast cancer. *Int J Pharm*. 2018;546(1–2):61–69. doi:10.1016/j.ijpharm.2018.05.032
15. Cui D, Xu D, Yue S, et al. Recent advances in the pharmacological applications and liver toxicity of triptolide. *Chem Biol Interact*. 2023;382:110651. doi:10.1016/j.cbi.2023.110651
16. Liu Q. Triptolide and its expanding multiple pharmacological functions. *Int Immunopharmacol*. 2011;11(3):377–383. doi:10.1016/j.intimp.2011.01.012
17. Park H, Otte A, Park K. Evolution of drug delivery systems: from 1950 to 2020 and beyond. *J Control Release*. 2022;342:53–65. doi:10.1016/j.jconrel.2021.12.030
18. Zhao Z, Ukidve A, Kim J, Mitragotri S. Targeting strategies for tissue-specific drug delivery. *Cell*. 2020;181(1):151–167. doi:10.1016/j.cell.2020.02.001
19. Zheng X-C, Ren W, Zhang S, et al. The theranostic efficiency of tumor-specific, pH-responsive, peptide-modified, liposome-containing paclitaxel and superparamagnetic iron oxide nanoparticles. *Int J Nanomed*. 2018;13:1495–1504. doi:10.2147/IJN.S157082

20. Cummings M, Freer C, Orsi N. Targeting the tumour microenvironment in platinum-resistant ovarian cancer. In: *Seminars in Cancer Biology*. Elsevier; 2021:3–28.
21. Zhou D, Duan Z, Li Z, Ge F, Wei R, Kong L. The significance of glycolysis in tumor progression and its relationship with the tumor microenvironment. *Front Pharmacol*. 2022;13:1091779. doi:10.3389/fphar.2022.1091779
22. Roma-Rodrigues C, Mendes R, Baptista PV, Fernandes AR. Targeting Tumor Microenvironment for Cancer Therapy. *Int J Mol Sci*. 2019;20 (4):840. doi:10.3390/ijms20040840
23. Zhang J, Li Y, Liu H, et al. Genome-wide CRISPR/Cas9 library screen identifies PCMT1 as a critical driver of ovarian cancer metastasis. *J Exp Clin Cancer Res*. 2022;41(1):24. doi:10.1186/s13046-022-02242-3
24. Carey P, Low E, Harper E, Stack MS. Metalloproteinases in ovarian cancer. *Int J Mol Sci*. 2021;22(7):3403. doi:10.3390/ijms22073403
25. Jo G, Kim EJ, Park MH, Hyun H. Tumor targeting with methotrexate-conjugated zwitterionic near-infrared fluorophore for precise photothermal therapy. *Int J Mol Sci*. 2022;23(22):14127. doi:10.3390/ijms232214127
26. Kansara V, Paturi D, Luo S, Gaudana R, Mitra AK. Folic acid transport via high affinity carrier-mediated system in human retinoblastoma cells. *Int J Pharm*. 2008;355(1–2):210–219. doi:10.1016/j.ijpharm.2007.12.008
27. Song L, Pan Z, Zhang H, et al. Dually folate/CD44 receptor-targeted self-assembled hyaluronic acid nanoparticles for dual-drug delivery and combination cancer therapy. *J Mat Chem B*. 2017;5(33):6835–6846. doi:10.1039/C7TB01548H
28. Ianevski A, Giri AK, Aittokallio T. SynergyFinder 3.0: an interactive analysis and consensus interpretation of multi-drug synergies across multiple samples. *Nucleic Acids Res*. 2022;50(W1):W739–W743. doi:10.1093/nar/gkac382
29. Han M, Ji X, Li J, et al. Lipoprotein-inspired nanocarrier composed of folic acid-modified protein and lipids: preparation and evaluation of tumor-targeting effect. *Int J Nanomed*. 2020;Volume 15:3433–3445. doi:10.2147/IJN.S241448
30. DeCarlo A, Malardier-Jugroot C, Szewczuk MR. Folic acid-functionalized nanomedicine: folic acid conjugated copolymer and folate receptor interactions disrupt receptor functionality resulting in dual therapeutic anti-cancer potential in breast and prostate cancer. *Bioconjugate Chem*. 2021;32(3):512–522. doi:10.1021/acs.bioconjchem.0c00625
31. Crowley LC, Marfell BJ, Waterhouse NJ. Analyzing cell death by nuclear staining with Hoechst 33342. *Cold Spring Harbor Protocols*. 2016;2016 (9):pdb.prot087205. doi:10.1101/pdb.prot087205
32. Luo Q, Wang J, Zhao W, et al. Vasculogenic mimicry in carcinogenesis and clinical applications. *J Hematol Oncol*. 2020;13:1–15. doi:10.1186/s13045-020-00858-6
33. Wang X, Lv Q, Meng Z. Analysis of the related influencing factors of hepatic abscess associated with hepatobiliary ischemic necrosis after cholangiocarcinoma operation. *Cell Mol Biol*. 2023;69(5):87–93. doi:10.14715/cmb/2023.69.5.15
34. Wang CZ, Yang SF, Xia Y, Johnson KM. Postnatal phencyclidine administration selectively reduces adult cortical parvalbumin-containing interneurons. *Neuropsychopharmacology*. 2008;33(10):2442–2455. doi:10.1038/sj.npp.1301647
35. Menon SS, Guruvayoorappan C, Sakthivel KM, Rasmi RR. Ki-67 protein as a tumour proliferation marker. *Clin Chim Acta*. 2019;491:39–45. doi:10.1016/j.cca.2019.01.011
36. Pastushenko I, Blanpain C. EMT transition states during tumor progression and metastasis. *Trends Cell Biol*. 2019;29(3):212–226. doi:10.1016/j.tcb.2018.12.001
37. Xue W, Yang L, Chen C, Ashrafizadeh M, Tian Y, Sun R. Wnt/beta-catenin-driven EMT regulation in human cancers. *Cell Mol Life Sci*. 2024;81 (1):79. doi:10.1007/s00018-023-05099-7
38. Zhao X, Ren T, Li S, et al. A new perspective on the therapeutic potential of tumor metastasis: targeting the metabolic interactions between TAMs and tumor cells. *Int J Biol Sci*. 2024;20(13):5109–5126. doi:10.7150/ijbs.99680
39. Gerber TS, Ridder DA, Schindeldecker M, et al. Constitutive occurrence of E:N-cadherin heterodimers in adherens junctions of hepatocytes and derived tumors. *Cells*. 2022;11(16):2507. doi:10.3390/cells11162507
40. Jiang X, Wang J, Deng X, et al. The role of microenvironment in tumor angiogenesis. *J Exp Clin Cancer Res*. 2020;39(1):204. doi:10.1186/s13046-020-01709-5
41. Shaw P, Dwivedi SKD, Bhattacharya R, Mukherjee P, Rao G. VEGF signaling: role in angiogenesis and beyond. *Biochim Biophys Acta Rev Cancer*. 2024;1879(2):189079. doi:10.1016/j.bbcan.2024.189079
42. Zhang M, Chen Y, Liu Z, Liu M, Wang Q. Series of desloratadine Platinum(IV) hybrids displaying potent antimetastatic competence by inhibiting epithelial–mesenchymal transition and arousing immune response. *J Med Chem*. 2024;67(3):2031–2048. doi:10.1021/acs.jmedchem.3c01845